A Thesis for the Degree of Doctor of philosophy in Pharmacology

Neuroprotection effects of Cudraisoflavones and extracts from the fruit of *Maclura tricuspidata* against *in vitro* and *in vivo* brain ischemic injury models via induction of microRNAs targeting Nox4 mRNA.

Nox4 mRNA 를 표적으로하는 miRNA 의 유도를 통한 꾸지뽕나무 열매 추출물과 분리된 컴파운드의 허혈성 손상 세포 및 동물에서의 모델에 대한 신경 보호 효과

August, 2017

By

Sungeun Hong

Natural product Science Major, College of Pharmacy

Doctor course in the Graduate School

Seoul National University

Abstract

Neuroprotection effects of Cudraisoflavones and extracts from the fruit of *Maclura tricuspidata* against *in vitro* and *in vivo* brain ischemic injury models via induction of microRNAs targeting Nox4 mRNA

Sungeun Hong
Natural Products Science Major
College of Pharmacy
The Graduate School
Seoul National University

A brain ischemia is a type of stroke that occurs when insufficient blood flow to the brain. This leads to reperfusion injury as well as. Reperfusion injury is when there blood supply returns to the brain circulation results in inflammation and oxidation damage on brain cell. Many drugs are based on improvements in existing therapies or on an understanding of the molecular mechanisms involved in oxidative stress. Cerebral ischemia is the third leading cause of death in industrial countries. Therefore, it is important to develop new compounds that are effective for the treatment of cerebral ischemia.

This study evaluated the neuroprotective effects of *Maclura tricuspidata* fruits on the two experimental models of cerebral ischemic damage in *in vitro* model oxygen-glucose deprivation/reoxygenation (OGD/R) and *in vivo* model middle cerebral artery occlusion/reperfusion (MCAO/R) of cerebral ischemia. Also, the isolated compounds from *M.tricuspidata* friuits were investigated the protective effects in *in vitro* model of cerebral ischemia. 50% EtOH extract of *M. tricuspidata* fruits (FME50) inhibited OGD/R-induced neuronal cell death, ROS generation, and NADPH oxidase 4 (Nox4) expression via induction of Nox4-targeting miRNA-25, miRNA-92a, and miRNA-146a in SH-SY5Y cells. Also, FME50 suppressed OGD/R-induced activation of apoptosis signal-regulating kinase 1 (ASK1)- c-Jun N-terminal kinases1 (JNK1) / p38 mitogen-activated protein kinases (MAPK) signal cascade. Among nine isolates from FME50, cudraisoflavone I (CFI) and cudraisoflavone H (CFH) attenuated OGD/R-induced cell death, ROS generation, and Nox4 expression by regulating miRNA-25, miRNA-92a, and miRNA-146a expression. Furthermore, CFI and CFH inhibited MAPK signal cascade. Furthermore, FME50 significantly reduced the MCAO/R–induced brain infarct, Nox4 expression via induction of Nox4-targeting three miRNAs. Additionally, FME50 suppressed MCAO/R-induced MAPK signal pathway.

Taken together, these findings suggest that the neuroprotective effect of FME50 and two isolated compound CFI and CFH on neurotoxicity is in part due to the inhibition of NOX activity and ROS generation. These results demonstrate that FME50, CFI, and CFH exert neuroprotective effects via Nox4 inhibition by the induction of Nox4-targeting miRNAs and inhibition of MAPK signal cascade, suggesting that they might be possible candidates for the treatment of cerebral ischemia.

Keywords: *Maclura tricuspidata*, MiroRNAs, Oxygen-glucose deprivation/reoxygenation, Middle cerebral artery occlusion/reperfusion, NADPH oxidase, MAPkinase

Student number : 2014-30572

Table of Contents

List of Tables

List of Figures

Abbreviations

FME50	50% EtOH extract of *Maclura tricuspidata* fruits
CFI	Cudraisoflavone I
CFH	Cudraisoflavone H
Nox	NADPH oxidase
OGD/R	Oxygen-glucose deprivation/reoxygenation
MCAO/R	Middle cerebral artery occlusion/reperfusion
MAPK	Mitogen-activated protein kinases
ASK1	Apoptosis signal-regulating kinase 1
JNK1	c-Jun N-terminal kinases1
P38	Mitogen-activated protein kinase
ROS	Reactive oxygen species
UPLC	Ultra performance liquid chromatography
SH-SY5Y	Neuroblastoma cell line

1. Introduction

Maclura tricuspidata Carrière (formerly known as *Cudrania tricuspidata*, Moraceae) is a tree widespread in Korea, China, and Japan and the ripe fruits can be eaten by hand or commercially used as pies, sherbets, tarts and wines. *M. tricuspidata* contains prenylated isoflavonoids, benzylated flavonoids, xanthones, quercetin and kaempferol (Hiep et al., 2015a; Han et al., 2009; Lee et al., 1995; Lee et al., 1996; Kim et al., 2009) and it showed anti-atherosclerotic and anti-inflammatory (Park et al., 2006), hepatoprotective (Tian et al., 2005), neuroprotective (Jeong et al., 2010), pancreatic lipase inhibitory (Jeong et al., 2014), antihypertensive (Kang et al., 2002), and antiallergic activities (Lee et al., 2015). Cudraisoflavone I (CFI) and cudraisoflavone H (CFH) from the fruit of *M. tricuspidata* were previously reported to have neuroprotective effects against 6-hydroxydopamine-induced cell death in SH-SY5Y cell (Hiep et al., 2015a).

Cerebral reperfusion injury initially caused by ischemia is due to insufficient blood supply to the brain, and this leads to poor oxygen supply and eventually neuronal cell death. After the ischemic period, reperfusion or reoxygenation is essential for survival of neuronal cells. However, the restoration of blood circulation results in the overproduction of mitochondrial reactive oxygen

species (ROS) in neuronal cells, and thereby implicates the cellular damage during neurological diseases, such as stroke (Chouchani et al., 2014). Oxidative stress plays a major role in the pathogenesis of neurological disorders, such as cerebral ischemia. Many studies have shown that oxidative stress plays a pathological role in cerebral ischemia (Chan, 2001). These post-ischemia oxidation reactions result in the overproduction of ROS in neuronal cells (Perjes et al., 2012). And the overproduction of intracellular ROS is an important factor to the pathogenesis of neurodegenerative disease of ischemia (Mei Jin et al., 2014. The majority of studies on the generation of ROS in brain ischemia have focused on the effects of mitochondrial dysfunction (Niizuma et al., 2010). Recently, attention has focused on the role of nicotinamide adenine dinucleotide phosphate (NADPH) oxidase (NOX) (Youn et al., 2013).

NOX4, a NOX family of ROS-generating NADPH oxidases, is widely expressed in neurons, astrocytes, and microglia. When NOX4 expression is stimulated by external stress or brain injury, the cytosolic subunits migrate to the plasma membrane and form a functional complex with p22phox to generate ROS (Bedard and Krause, 2007). Recent studies suggest that ROS generated via the NOX family plays a major role in neurodegenerative diseases, such as cerebral ischemia (Sorce and Krause, 2009). It was reported

that the mitochondrial ROS can be formed by xanthine oxidase, cytochrome P450, nitric oxide synthase, and nicotinamide adenine dinucleotide phosphate oxidase (Nox). Human genome encodes seven members of the Nox family (Nox1 - Nox5, Duox1 and Duox2), and Nox is a membrane-bound enzyme complex composed of six subunits with different patterns of expression (K., 2011). When Nox4 expression is stimulated by external stress or brain injury, the integral membrane protein $p22^{phox}$ forms a heterodimeric functional complex with Nox4 to generate ROS (Bedard and Krause, 2007), suggesting that ROS generated by the Nox4 activation plays a major role in cerebral ischemia. Recent studies reported that Nox activity is connected with Nox targeting miRNAs expression (Liu et al., 2016).

MiRNAs are small noncoding RNAs with 19-25 nucleotides and regulates the basis cellular functions such as proliferation, differentiation, and death (Hwang and Mendell, 2006). MiRNAs are known to play an important role in many pathological processes in the brain (Adlakha and Saini, 2014) and some miRNAs are expressed in neuronal cell. Among them, three different miRNAs (miRNA-25, miRNA-92a, and miRNA-146a) are highly related in the regulation of Nox4 mRNA expression (Fu et al., 2010; Wang et al., 2014; Tsao et al., 2015). These miRNAs modulate protein expression by binding

complementary target mRNA and the target mRNA degradation or translational inhibition are occur (Jeyaseelan et al., 2008). It was reported that silencing of Nox4 mRNA expression inhibited ROS production (Wang et al., 2014) and inhibited hypoxia-induced activation of apoptotic signals such as ASK1, JNK, and p38 (Mkaddem et al., 2010). Ischemia-induced ROS attributes in part to the activation of mitogen-activated protein kinases (MAPK).

Apoptosis signal-regulating kinase 1 (ASK1) is an upstream regulator of MAPK cascade and activated by various stresses including oxidative stress, ER stress, calcium influx, receptor-mediated inflammatory signals and ischemic injuries (Ichijo et al., 2007). ASK1 activates c-Jun N-terminal kinases 1 (JNK1), known as a mediator of neuronal degeneration in response to stress, and phosphorylated p38 mitogen-activated protein kinase, one of apoptosis factors related MAPK (Irving and Bamford, 2002). The JNK1 was known to bind and phosphorylate the DNA binding protein c-Jun and elevate its transcriptional activity and the p38 kinase was expressed in most cell types and regulated of many cytokines. Inhibition of these proteins are cell survival and thereby MAPK pathway targets for drug development (Johnson and Lapadat, 2002).

Previously, we reported that isoflavones and extracts from fruits of *M. tricuspidata* exerted the neuroprotective effects against 6-OHDA-induced in cell death (Hiep et al., 2015a; Kim et al., 2017). In this stiudy, we investigated the neuroprotective effect of different extracts (0 – 100% ethanol ratio) and nine isoflavones from *M. tricuspidata* fruits in *in vitro* and *in vivo* models of cerebral ischemia. Our studies focused on the inhibition of intracellular ROS generation, Nox4 expression, induction of miRNAs (miRNA-25, miRNA-92a, and miRNA-146a) targeting Nox4 mRNA expression, and inhibition of apoptosis via ASK1-JNK/p38 MAPK signal cascade using oxygen-glucose deprivation/reoxygenation (OGD/R) *in vitro* model, and middle cerebral artery occlusion/reperfusion (MCAO/R) *in vivo* model of cerebral ischemia.

2. Materials and Methods

2.1. Chemicals and reagents

2',7'-dichlorfluorescein-diacetate (DCFH-DA), carnosine, and VAS2870 (a NOX inhibitor), were purchased from Sigma-Aldrich (St. Louis, MO, USA). Dulbecco's modified Eagle's medium (DMEM) and fetal bovine serum (FBS) were purchased from Hyclone™ Thermo scientific (Wyman Street Waltham, MA, **USA**). Hybond-polyvinylidene difluoride (PVDF) membrane purchased from Amersham Pharmacia Biotechnology Inc. (Piscataway, NJ, USA). Easy-Blue® total RNA extraction solution, One Step RT-PCR Premix Kits, PRO-PREP protein extraction solution and WEST-ZOL® ECL solution were purchased from iNtRON Biotechnology (Kyunggi, Korea). Nox4, ASK1, p-ASK1, JNK1, p38, p-p38, β-actin primary antibody and secondary antibody purchased from Santa Cruz Biotechnology, Inc. (CA, U.S.A.). The miRNAs mimic and inhibitor (miRNA-25, miRNA-92a, miRNA-146a) were purchased from Applied Biosystems (Foster City, CA, USA).

2.2. UPLC chromatogram of 50% EtOH extract from *Maclura*

***tricuspidata* fruits (FME50)**

All samples were analyzed using an Acquity UPLC system (Waters, Millford, MA, USA) equipped with an Acquity BEH C18 column (2.1 mm × 150 mm i.d., 1.7 μm). The mobile phases were consisted of 0.05% formic acid in water (A) and acetonitrile (B), with a flow rate of 0.3 mL/min. The initial eluent was 35% B, and its proportion was increased linearly to 95% B until 10 min, held constant at 100% until 11.5 min, returned to the initial composition at 10.5 min, and then held constant for 1.5 min to re-equilibrate the column. The sample injection volume was 4 μL for extracts and 2 μL for compounds. The column and sample managers were set at 35 and 15 °C, respectively, and the UV wavelength was monitored at 265 nm.

2.3. Plant material and sample preparation

The fruits of *Maclura tricuspidata* were collected from the Korea Forest Research Institute, Southern Forest Research Center (Jinju, Korea). A voucher specimen (accession no. KH1-5-090904) was deposited at the Department of Biosystems and Biotechnology, Korea University (Seoul, Korea). The dried fruits of *M. tricuspidata* (3.4kg, yield 18.88%, w/w) were ground and sifted

through a 120-mesh sieve. The partial of samples (7.0 g) were refluxed three times by means of heating mantle with 250 mL of each 0, 30, 50 70, and 100% ethanol for 1h. Each extract was combined, filtered, and concentrated in vacuo to obtain various samples (2.85 g, 2.71 g, 2.58 g, 2.67 g, and 2.15 g, respectively). The chemical investigation led to the isolation of nine isoflavones, namely, cudraisoflavone I (**1**, 0.0007%), cudraisoflavone H (**2**, 0.0013%), gancaonin A (**3**, 0.0086%), 6,8-diprenylorobol (**4**, 0.0015%), alpinumisoflavone (**5**, 0.0762%), 4′-*O*-methylalpinumisoflavone (**6**, 0.0046%), 6,8-diprenylgenistein (**7**, 0.0055%), isoerysenegalensein E (**8**, 0.0221%), and erysenegalensein E (**9**, 0.0181%). Their structures were identified by interpretation of spectroscopic data, and the purity of each compound was more than 95%. Fresh fruits of *Maclura tricuspidata* (10.7 kg) were dried, ground, and extracted with EtOH (3 × 10.0 L) at room temperature, in 10 days. The extracts were evaporated in vacuo to afford a EtOH extract (TH1-1-1, 630.9 g), which was then suspended in H_2O (2 × 2.5 L). The aqueous solution was partitioned with *n*-hexane (4 × 2.0 L) and EtOAc (5 × 2.0 L) to give *n*-hexane (TH1-2-1, 48.4 g) and EtOAc (TH1-2-2, 27.8 g) soluble extracts. The EtOAc soluble extract was firstly fractionated by silica gel column chromatography (CC) using a $CHCl_3$–EtOH gradient system (1:0 to 1:1) to yield six fractions (TH1-4-1–TH1-4-6). Fraction TH1-4-3 (9.68 g)

was subjected to silica gel CC with a gradient system of *n*-hexane–EtOAc (1:0 to 0:1) to give seven subfractions (TH1-10-1–TH1-10-7). Fraction TH1-10-4 (4.7 g) was further isolated by silica gel CC with a gradient mixture of *n*-hexane–$CHCl_3$–EtOH (1:0:0 to 0:1:1), resulting in sixteen subfractions (TH1-74-1–TH1-74-16). Fraction TH1-74-4 (1.4 g) was separated by Sephadex LH-20 CC eluted with $CHCl_3$–EtOH (1:1) to yield eight subfractions (TH1-84-1–TH1-84-8). Fraction TH1-84-4 (552.0 mg) was separated using Sephadex LH-20 CC with $CHCl_3$–EtOH (1:1), producing six subfractions (TH1-104-1–TH1-104-6). Fraction TH1-104-4 (191.7 mg) was purified by preparative HPLC (EtOH–H_2O, 50–90% EtOH in H_2O) to afford 6,8-diprenylgenistein (**7**, 4.0 mg) (Sekine et al., 1999). TH1-74-12 (166.3 mg) was fractionated by RP C_{18} silica gel CC with a gradient system of EtOH–H_2O (1:1 to 1:0) to give six subfractions (TH3-9-1 – TH3-9-6). Fraction TH3-9-1 (71.0 mg) was then separated by silica gel CC with a gradient mixture of *n*-hexane–EtOAc (1:0 to 0:1), resulting in the preparation of five fractions (TH3-19-1 – TH3-19-5). Fraction TH3-19-3 (40.5 mg) and TH3-19-4 (12.3 mg) were purified by preparative HPLC (EtOH–H_2O, 60–81% EtOH in H_2O), leading to the isolation of cudraisoflavones H (**2**, 4.2 mg)(Hiep et al., 2015b) and I (**1**, 5.8 mg) (Hiep et al., 2015b). Fraction TH1-10-5 (909.3 mg) was separated by Sephadex LH-20 CC eluted with $CHCl_3$–EtOH (1:1) to yield

seven subfractions (TH3-51-1–TH3-51-7). Fraction TH3-51-5 (311.3 mg) was fractionated by silica gel CC using a gradient mixture of *n*-hexane–EtOAc (1:0 to 0:1), producing eight fractions (TH3-69-1–TH3-69-8). Fraction TH3-69-3 (95.3 mg) was subjected to silica gel CC with a gradient system of *n*-hexane–EtOAc (1:0 to 0:1) to yield six subfractions (TH3-79-1–TH3-79-6). Furthermore, the first fraction (29.3 mg) was purified by preparative HPLC (EtOH–H_2O, 60–95% EtOH in H_2O), leading to isolation of alpinumisoflavone (**5**, 2.9 mg) (Hiep et al., 2015b) and gancaonin A (**3**, 2.8 mg)(Hiep et al., 2015b). Fraction TH3-79-4 (51.2 mg) was further separated by preparative HPLC (EtOH–H_2O, 60–95% EtOH in H_2O) to afford isoerysenegalensein E (**8**, 40.3 mg) (Hiep et al., 2015b). The purification of fraction TH3-69-5 (64.6 mg) was carried out by preparative HPLC (EtOH–H_2O, 65–95% EtOH in H_2O), leading to the isolation of erysenegalensein E (**9**, 38.6 mg)(Hiep et al., 2015b). Fraction TH1-10-6 (1672.0 mg) was fractionated by Sephadex LH-20 CC with $CHCl_3$–EtOH (1:1), resulting in eleven subfractions (TH3-101-1–TH3-101-11). Fraction TH3-101-8 (243.8 mg) was eluted on silica gel CC with *n*-hexane–EtOAc gradient system (1:0 to 0:1), leading to preparation of five fractions (TH3-129-1–TH3-129-5). The purification of first fraction (16.7 mg) was carried out by semipreparative HPLC (EtOH–H_2O, 60–85%, EtOH in H_2O), to give 4′-*O*-

methylalpinumisoflavone (**6**, 2.1 mg)(Olivares et al., 1982). Fraction TH1-4-4 (2.30 g) was separated using Sephadex LH-20 CC with $CHCl_3$–EtOH (1:1) to yield eight subfractions (TH4-21-1–TH1-21-8). Fraction TH4-21-7 (757.8 mg) was applied to silica gel CC eluted with gradient mixture of $CHCl_3$–EtOH (1:0 to 1:1), resulting in the preparation of 10 fractions (TH4-77-1–TH3-77-10). Fraction TH4-77-4 (76.4 mg) was purified by preparative HPLC (EtOH–H_2O, 50–95%, EtOH in H_2O) to obtain 6,8-diprenylorobol (**4**, 26.9 mg) (Wang et al., 2013).

2.4. SH-SY5Y cell culture

The human neuroblastoma cell line SH-SY5Y (ATCC No. CRL-2266) was purchased from the American Type Culture Collection (Manassas, VA, USA) and cultured in DMEM supplemented with 10 % heat-inactivated FBS and 1 % penicillin/streptomycin at 37 ºC in a humidified atmosphere of 95% air and 5 % CO_2.

2.5. Treatment of samples in oxygen-glucose deprivation/reoxygenation (OGD/R) model

Briefly, SH-SY5Y cells were seeded at a density of 1×10^5 cells/200 μL/well in 96-well plates for 24 h, and then cells were treated with FME50 (0.08 - 2 μg/mL), CFI, CFH and VAS2870 (0.016 - 4 μM), or vehicle and simultaneously OGD/R was performed as described previously (Hong et al., 2017). Briefly, after treatment of samples, cells were incubated in a hypoxia chamber (Modular Incubator Chamber MIC-101, Billups-Rothenberg, Del Mar, CA) containing a mixture of 95% N_2 and 5% CO_2 at 37 °C for 16 h. After hypoxia, reoxygenation and glucose restoration were performed for an additional 24 h. In the normoxia control group, cells were cultured with DMEM containing glucose under normal conditions (5% CO_2 at 37°C for 16 h).

2.6. Measurement of cell viability

Cell viability was evaluated using MTT assay as previously described with a slight modification (Ghaffari et al., 2014a). Briefly, cell viability was determined by MTT dissolved in PBS (0.5 mg/mL) at 37 °C for 4 h. The formazan crystals were dissolved with dimethyl sulfoxide (DMSO). The number of viable cells was measured at 540 nm with a microplate reader (SpectraMax®M5, Molecular Devices, Sunnyvale, CA, USA).

2.7. Measurement of intracellular ROS

SH-SY5Y cells were plated into 6-well plates at a density of 2×10^5 cells/2 ml/well for 24 h and then cell treated with carnosine (0.08, 0.4 and 2 μM), or vehicle and then exposed to OGD/R condition. ROS were measured with 2',7'-dichlorofluorescein diacetate (DCFH-DA), as previously described (Kim et al., 2015). Briefly, cells were washed 3 times with PBS and incubated with DCFH-DA (4 μM) for 30 minutes at 37 ºC in the dark, then washed 3 times with PBS. Approximately $1x10^4$ cells were used for each experiment and the fluorescence intensities were measured by flow cytometry (BD FACSCalibur ™).

2.8. Measurement of Nox enzymatic activity in SH-SY5Y cells

SH-SY5Y cells were plated into 6-well plates at a density of 2×10^5 cells/2 ml/well for 24 h and then cells were treated with of FME50 (0.08, 0.4, and 2 μg/mL) and CFI, CFH, or a NOX inhibitor VAS2870, and vehicle (0.016, 0.8, and 4μM) and simultaneously exposed to OGD/R condition. Nox activity was determined by lucigenin chemiluminescence assay, as described previously

(Lo et al., 2013). Briefly, SH-SY5Y cells were homogenized with a sonicator (Vibra cell-VCX130) in PRO-PREP® protein extraction solution (iNtRON Biotechnology, Korea). The reaction mixture (10 μM lucigenin, 150 mM EGTA, 50 mM sucrose, 100 μM NADPH) in 96-well white plate. The reaction performed in the dark for 5 minutes at room temperature. (Wissing and Smith, 2000). The mean chemiluminescence observed by luminometer over 200 s in a scintillation counter (Centro LB 960, Berthold Technologies) at 5-s intervals and was calculated by subtracting the background values from those in the production of O^2. The light emission was detected at 506nm (Lopez-Sepulveda et al., 2011).

2.9. Transfection of miRNA and RNA preparation

SH-SY5Y cells were plated into 12-well culture plates at a density of 1.0×10^5 cells/1 mL/well for 24 h and then cells were transfected with 200 nM of miRNA-25, miRNA-92a, miRNA-146a, and 200 nM of inhibitor miRNA-25, miRNA-92a, and miRNA-146a for 48 h in lipofectimine-2000 (Invitrogen, Carlsbad, CA). Moreover, samples and, a NOX inhibitor, VAS2970 (0.016 - 4μM), or vehicle were treated and exposed to OGD/R condition. Total RNA was extracted from cells by Easy-Blue®. Briefly, RNA extraction were

centrifuged at 13,000×g for 15 minutes at 4°C and added DEPC-treated water to the RNA pellet. The purity and concentration of RNA were determined using NanoDrop 1000 spectrophotometer (Thermo Scientific, Wilmington, DE, USA). The pellet was used as the total RNA extract for qRT-PCR.

2.10. Determination of Nox4 mRNA expression by quantitative RT-PCR (qRT-PCR)

The total RNA (1 μg) was reverse transcribed to cDNA using cDNA synthesis Kit (with oligo(dt) 2X) (GeNet Bio, Cheonan, Korea). The cDNA amplify was performed using a Thermo Cycler PCR system 2720 (Applied Biosystems, Carlsbad, U.S.A.). The reaction were performed with a TOpreal^{TM} qPCR 2X PreMix (SYBR Green with high ROX) (Enzynomics, Hanam, Korea) using Thermo cycler Real-Time PCR systems 7300 (Applied Biosystems, Carlsbad, CA, USA). The PCR amplification was performed with following conditions: 10 min at 95 ˚C, 45 cycles of 95˚C for 20s, 60˚C for 30s and 72 ˚C for 30s. The primers used were as follows:

Nox4 forward: 5′-CTCAGCGGAATCAATCAGCTGTG-3′,

Nox4 reverse: 5′-AGAGGAACACGACAATCAGCCTTAG-3′ (Pedruzzi et al., 2004),

β-actin forward: 5′-GACCCAGATCATGTTTGAGA-3′,

β-actin reverse: 5′-GCTTGCTGATCCACATCTGC- 3′ (Hiney et al., 2010). Relative expression was calculated using a normalized ratio to the average Ct value of the β-actin (Farago et al., 2008) .

2.11. Determination of miRNAs by quantitative RT-PCR (qRT-PCR)

The miRNA reverse transcription reaction was performed with the Taqman®MicroRNA Reverse Transcription Kit (Applied Biosystems, CA, USA). Total RNA (350ng) from each treatment was reverse transcribed in the presence of 5×RT TaqMan® MicroRNA Assays kit (Applied Biosystems, CA, USA). Reaction mixture (8µl) contains 2.0 µl of dNTPs, 1.5µl of MultiScribe™ Reverse Transcriptase (50 U/µl), 0.8 µl of 10 X RT Buffer, 0.9 of µl $MgCl_2$, 0.1 µl of RNase inhibitor (20 U/µl), 1.5 µl of 5 X RT primer. The expression level of miRNAs was determined with 7300 Real-Time PCR systems (Applied Biosystems, Carlsbad, CA, USA). Reverse Transcription was carried out with the following cycling: 16°C for 2 min, 42°C for 1 min, 50°C for 1 min, 50°C for 1 sec, 45 cycles, and then samples were hold at 85°C for 5 min.

2.12. Protein Extraction

SH-SY5Y cells were plated into 60π dishes at a density of 2.0×10^5 cells/4 mL/well for 24 h with OGD/R condition. Protein was extracted with PRO-PREP protein extraction solution (iNtRON Biotechnology, Korea) for 20 minutes at -20 °C. Lysates were centrifuged at 13,000×g for 10 minutes at 4 °C and the supernatant was used for western blot analysis.

2.13. Western blot assay

Briefly, the protein was determine by Bradford assay (Jones et al., 1989), and equal amount of protein (15 μg) were electrophoresed by SDS-PAGE on a 10% gel, transferred to a PVDF membrane for 2 h, and then blocked with 5% skim milk in TBST for 2 h at room temperature. The membrane was incubated overnight at 4 °C with a primary antibody (Nox4, ASK1, p-ASK1, JNK, p-JNK, p38, p-p38, cleaved caspase3, and caspase3 were diluted 1:2000, and β-actin was diluted 1:5000) followed by incubation with a secondary antibody (anti-rabbit or anti-mouse HRP-conjugated IgG was diluted 1:5000) for 1 h at room temperature. The band intensity was detected using ImageQuant™ LAS

4000 (GE Healthcare Life Science, USA) image analyzer. The membrane was stripped and reprobed with anti-β-actin antibody as an internal control as previously described (Ham et al., 2013).

2.14. Animals

Male Sprague-Dawley rats were purchased from Samtako Bio Korea (Osan, Korea) and housed in groups (2~3 rats/cage) for experiment. The environment was maintained at 60% humidity with a 12/12-light-dark cycle and unlimited access to food and water. Male Sprague-Dawley rats 6-7 weeks after birth (200-210 g) were used. All animal experiments were approved by the Institutional Animal Care and Use committee of Seoul Nation University and performed in accordance with the requirements of European Directive 2010/63/EU. All efforts were made to minimize the number of animals used and their pain. After each experiment, animals were euthanized by an overdose of anesthetics.

2.15. Application of FME50 for Animals

The FME50 and carnosine, a control compound, were dissolved in saline, and administered orally for once a day at a dose 25, 50 and 100 mg/kg of FME50

and 75, 150 and 300 mg/kg of carnosine for 7 days. The animals were divided into 4 groups of 6 rats including a sham surgery control, a vehicle-treated MCAO/R, a FME50-treated MCAO/R, and a carnosine-treated MCAO/R groups.

2.16. Middle cerebral artery occlusion/reperfusion (MCAO/R)

Rats were anesthetized with 2-3% isoflurane (Aerrane®) purchased from Baxter (Deerfield, Illinois, USA) in a mixture of 30% O_2 and 70% N_2O through a face mask during surgery. Body temperature was maintained at 37 ± 0.5°C with a heating pad. Focal cerebral ischemia was induced by intraluminal MCAO as previously described (Truong et al., 2012). In brief, the right external carotid artery (ECA), the common carotid artery (CCA), and the internal carotid artery (ICA) branches were separated from surrounding nerves and fascia. Then, the middle cerebral artery (MCA) was occluded with a 3-0 poly-L-lysine-coated nylon suture through the extracranial ICA for 2 h. Reperfusion was performed by removing the suture. The sham-operated control group received all surgical procedures except suture occlusion process. After the MCAO/R surgery, animals were provided unlimited access to food and water for 24 h and then euthanized.

2.17. Determination of infarct volume

To evaluate the infarct volume, the brains were carefully removed within 3 minutes of euthanasia. They were cut into five coronal sections of 2-mm thickness by rat brain matrix purchased from Harvard Bioscience (Holliston, MA, U.S.A.). The slices were placed in 24-well plates and stained with 2% 2, 3, 5-triphenyltetrazolium chloride (TTC) at 37 °C for 30 minutes, then fixed with 4% paraformaldehyde solution. The unstained white area of the brain slice was defined as the infarction, and the infarct volume ratio was measured and calculated using a computerized image analyzer using Image J Software (NIH, Maryland, USA) as previously described (Cho et al., 2010). Briefly, the percentage infarct volume was calculated as: $[(V_C - V_L)/V_C] \times 100$, where V_C is the volume of control hemisphere and V_L is the volume of non-infarcted tissue in the lesioned hemisphere.

2.18. RNA preparation from rat brain

For RNA preparation, extraction of total RNA was the purification of RNA from homogenized cortex by Easy-Blue®. RNA extraction were centrifuged at 13,000×g for 15 minutes at 4 °C and added DEPC treated water to the RNA

pellet. The purity and concentration of RNA were determined using NanoDrop 1000 spectrophotometer (Thermo Scientific, Wilmington, DE, USA). The total RNA extract was used as for qRT-PCR procedures.

2.19. Protein Extraction from rat brain

The homogenized cortex was lysed in PRO-PREP protein extraction solution (iNtRON Biotechnology, Korea) for 20 minutes at -20 °C. Lysates were centrifuged at 13,000×g for 10 minutes at 4 °C and the supernatant was used as the total brain protein extract for immunoblotting procedures.

2.20. Statistical analysis

All experimental data are expressed as the mean value ± standard deviation from three different experiments. Statistical significance between multiple groups was determined by one-way ANOVA (PRISM Graph Pad, San Diego, CA, USA). When ANOVA had a significant difference, *post hoc* Bonferroni's multiple comparison tests was conducted. *P* value less than 0.05 was regarded to be statistically significant.

3. Results

3.1. Neuroprotective effects of *M. tricuspidata* in SH-SY5Y cells

Ethanol is commonly used to extract bioactive compounds from plant materials. The ratio of water to ethanol can influence on the bioactivity of plant extracts (Ganora, 2009). We evaluated the neuroprotective effects of *M. tricuspidata* fruits and leaves extract (0, 30, 50, 70, and 100% ethanol) within nontoxic concentration ranges. As shown in Fig 1 and Table. 1, the extract of *M. tricuspidata* fruits showed potent protective effect with an EC_{50} 1.9 μg/mL.

(A)

Part of *Maclura tricuspidata*	Protective effect against OGD-induced cell death(EC_{50})
M. tricuspidata fruits (0% EtOH extract)	5.5 μg/mL
M. tricuspidata fruits (30% EtOH extract)	4.2 μg/mL
M. tricuspidata fruits (50% EtOH extract)	1.9 μg/mL
M. tricuspidata fruits (70% EtOH extract)	3.2 μg/mL
M. tricuspidata fruits (100% EtOH extract)	4.2 μg/mL
M. tricuspidata leaves (0% EtOH extract)	2.5 μg/mL
M. tricuspidata leaves (30% EtOH extract)	3.2 μg/mL
M. tricuspidata leaves (50% EtOH extract)	2.1 μg/mL
M. tricuspidata leaves (70% EtOH extract)	5.3 μg/mL
M. tricuspidata leaves (100% EtOH extract)	6.7 μg/mL

Table. 1. Neuroprotection of the percent of EtOH extracts from the fruits and leaves of *M. tricuspidata* against in ODG/R-induced SH-SY5Y cells

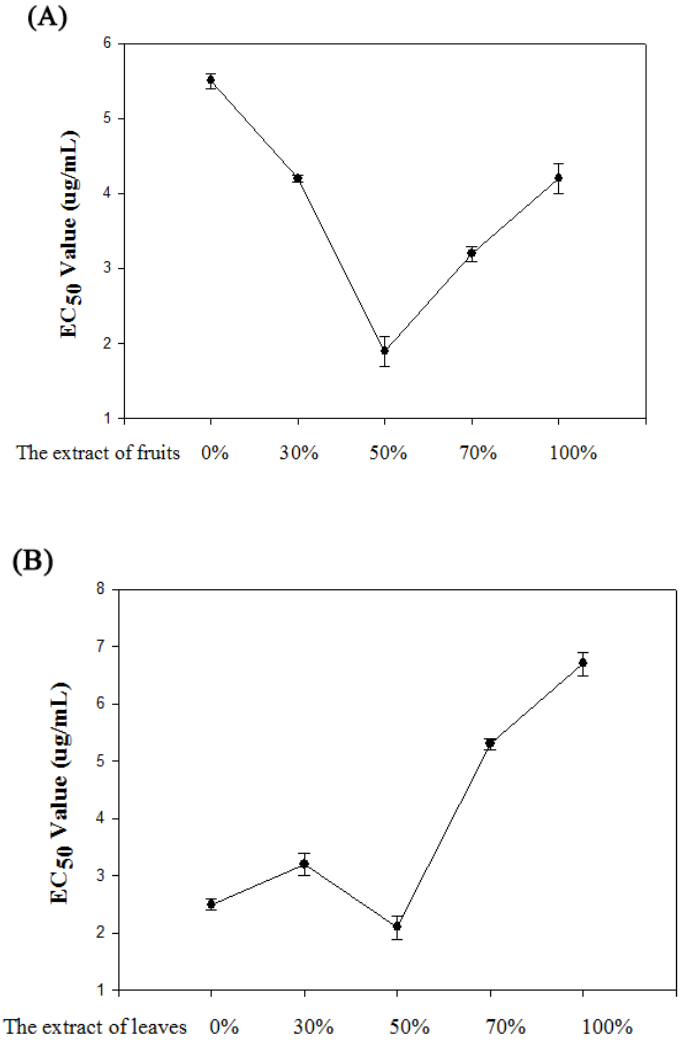

Fig. 1. The graph of neuroprotection of the percent of EtOH extracts from the fruits and leaves of *M. tricuspidata* against in ODG/R-induced SH-SY5Y cells

3.2. Protective effects against OGD/R-induced neuronal cell death in SH-SY5Y cells

The constituents of FME50 were identified using UPLC, and nine compounds were isolated (Fig. 3). As shown in Fig 2A and Table. 2, FME50 showed potent protective effect with an EC_{50} value of 1.9 μg/mL. Among nine isolated compounds from FME50, two isoflavone compounds (CFI and CFH) significantly attenuated OGD/R-induced neurotoxicity with EC_{50} values of 3.3 μM, and 11.4 μM, respectively (Fig. 2A and Table. 2), whereas the other compounds revealed no significant effects (Table. 2). The Nox inhibitor of VAS2870, a control compound, also protected neuronal cells with an EC_{50} of 0.48 μM (Fig. 2A and Table. 2).

(A)

	Inhibition effects of cell death (EC_{50})
(1) Cudraisoflavone I (CFI)	3.3 μM
(2) Cudraisoflavone H (CFH)	11.4 μM
(3) Gancaonin A	26.5 μM
(4) 6,8-Diprenylorobol	34.2 μM
(5) Alpinumisoflvone	>25 μM
(6) 4'-*O*-methylalpinumisoflavone	>25 μM
(7) 6,8-Dipreylgenistein	>25 μM
(8) Isoerysenegalensein E	>25 μM
(9) Erysenegalensein E	>25 μM
VAS2870 (positive control)	0.48 μM

Table. 2. Neuroprotection of isolated-compounds of *M. tricuspidata* against in ODG/R-induced SH-SY5Y cells. The values were determined in a semilogarithmic graph with 4 different concentrations of test materials. At least 3 independent experiments were performed. VAS2870, a Nox inhibitor, was used as a positive control compound.

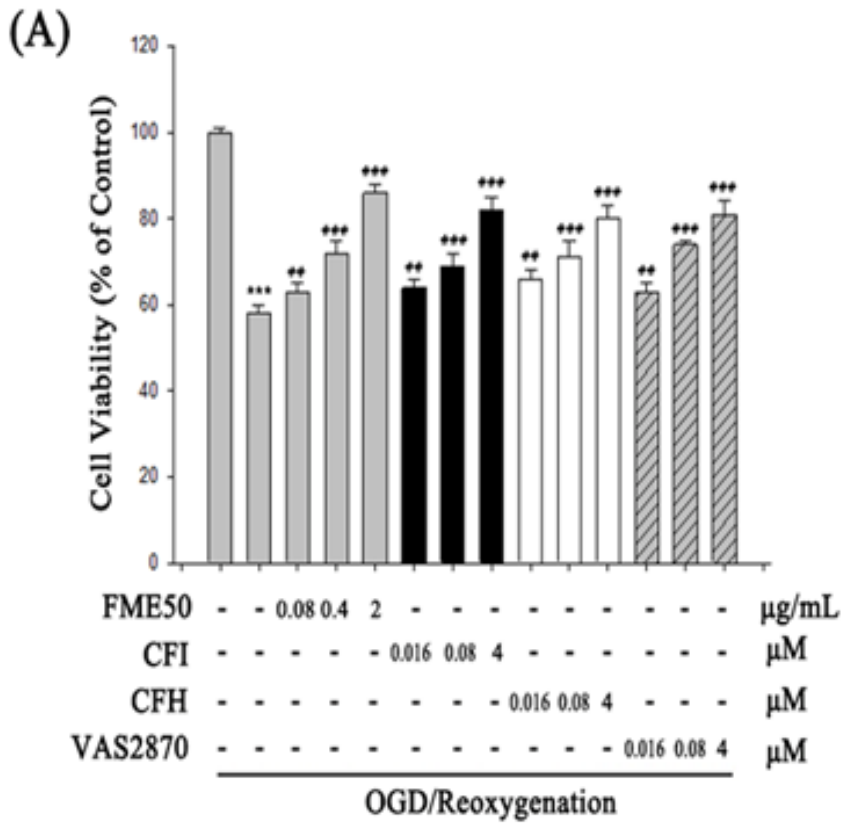

Fig. 2. The effect of FME50, CFI, CFH or VAS2870 on OGD/R-induced cell death in SH-SY5Y cells was measured by an MTT reduction assay. The cells were treated with different concentrations of FME50 (0.08 – 2 µg/ml) or VAS2870 (0.016 – 4 µM) and exposed to OGD/R conditions **(A).** Data represent the mean ± SD of three independent experiments. ($^{***}p<0.001$ compared to the control group, $^{\#}p<0.05$, $^{\#\#}p<0.01$ and $^{\#\#\#}p<0.001$ compared to the OGD/R-induced group).

(A)

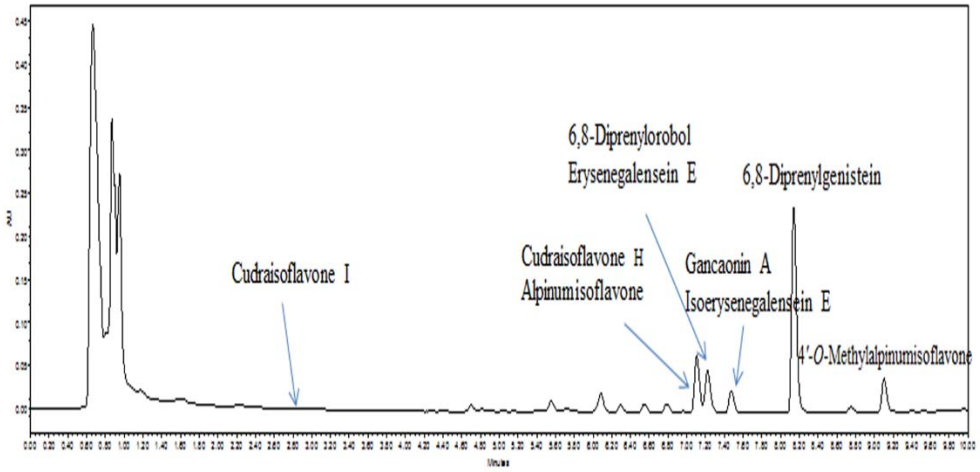

Fig. 3. Structures of the principal compounds and UHPLC chromatogram of FME50. (A) Chemical structures of principal compounds

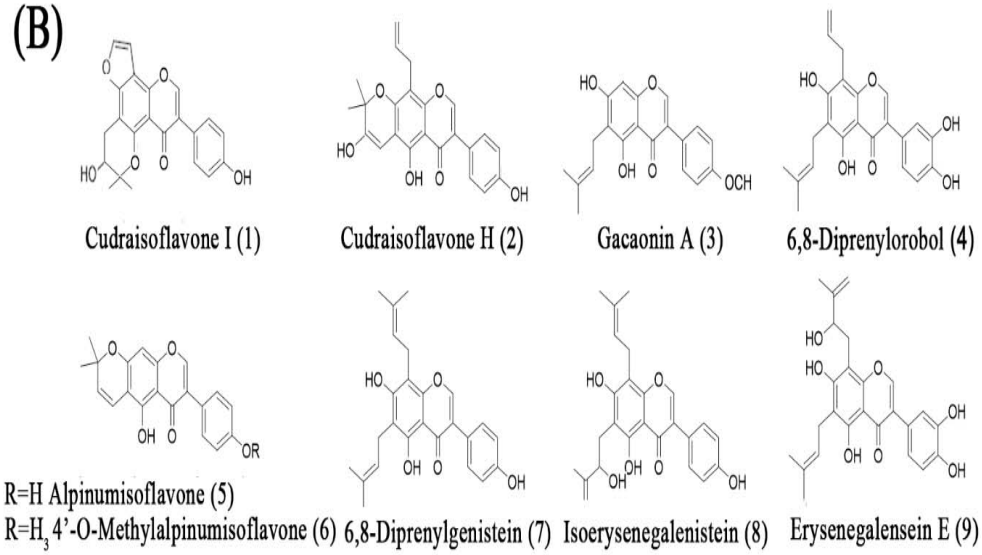

Fig. 4. (B) UHPLC chromatogram of FME50. The principal compounds are cudraisoflavone I (1), cudraisoflavone H (2), 5,7-dihydroxy-6-(2”-hydroxy-3”-methylbut-3”-enyl)-4'-methoxylisoflavone (3), gancaonin B (4), gancaonin A (5), lupiwighteone (6), and 6,8-diprenylorobol (7).

3.3. Inhibitory effects against OGD/R-induced intracellular ROS generation in SH-SY5Y cells

It has been reported that ROS generated by Nox enzyme induces neuronal cell death and is closely linked to cerebral ischemia (Nomura et al., 2004; Matsuzawa et al., 2002). As shown in Fig. 4B and Table. 3, FME50 showed the potent inhibition of OGD/R-induced ROS generation with an IC_{50} value of 3.5 μg/mL. Among the nine compounds derived from FME50, CFI and CFH showed a significant inhibitory effect against OGD/R-induced ROS generation with IC_{50} values of 5.8 μM, 13.3 μM, respectively (Fig. 4A and Table. 1). VAS2870 also inhibited ROS generation in OGD/R-induced SH-SY5Y with an IC_{50} values of 4.5 μM (Fig. 6A and Table 3.)

(A)

	Inhibition effects of ROS generation (IC_{50})
M. tricuspidata fruits (0% EtOH extract)	7.7 μg/mL
M. tricuspidata fruits (30% EtOH extract)	6.5 μg/mL
M. tricuspidata fruits (50% EtOH extract)	3.2 μg/mL
M. tricuspidata fruits (70% EtOH extract)	4.5 μg/mL
M. tricuspidata fruits (100% EtOH extract)	5.0 μg/mL
(1) Cudraisoflavone I (CFI)	5.3 μM
(2) Cudraisoflavone H (CFH)	13.3 μM
(3) Gancaonin A	31.6 μM
(4) 6,8-Diprenylorobol	30.3 μM
(5) Alpinumisoflvone	>25 μM
(6) 4'-*O*-methylalpinumisoflavone	>25 μM
(7) 6,8-Dipreylgenistein	>25 μM
(8) Isoerysenegalensein E	>25 μM
(9) Erysenegalensein E	>25 μM
VAS2870 (positive control)	1.3 μM

Table. 3. Neuroprotection of isolated-compounds of *M. tricuspidata* against inhibition of ROS generation in ODG/R-induced SH-SY5Y cells. The values were determined in a semilogarithmic graph with 4 different concentrations of test materials. At least 3 independent experiments were performed. VAS2870, a Nox inhibitor, was used as a positive control compound.

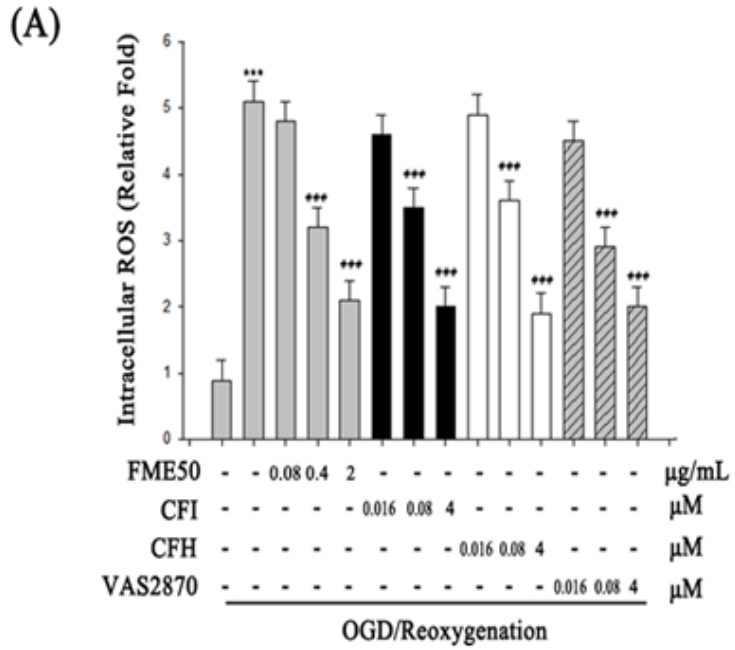

Fig. 5. The effects of FME50 on OGD/R-induced intracellular ROS generation in SH-SY5Y cells are illustrated by DCFH-DA staining. The cells were treated with different concentrations of FME50 (0.08 – 2 µg/ml) or VAS2870 (0.016 – 4 µM) **(A)** and exposed to OGD/R conditions. Data represent the mean ± SD of three independent experiments. ($^{***}p<0.001$ compared to the control group, $^{\#}p<0.05$, $^{\#\#}p<0.01$ and $^{\#\#\#}p<0.001$ compared to the OGD/R-induced group).

3.4. Inhibitory effects against OGD/R-induced Nox4 mRNA expression in SH-SY5Y cells

Nox4 is stimulated by external stress or brain injury generates ROS, suggesting that ROS generation by the Nox4 activation plays a key role in cerebral ischemia (Bedard and Krause, 2007). As shown in Fig. 6, OGD/R-induced cells exhibited the increase of Nox4 mRNA expression. When cells were treated with different concentrations of FME50 (0.08 – 2 μg/mL), CFI, and CFH (0.016 – 4 μM), the expression of Nox4 mRNA were decreased to normal in a concentration-dependent manner (Fig.6). FME50 (2 μg/mL), CFI, and CFH (4 μM) almost restored to normal state of Nox4 mRNA expression. Similarly, a Nox inhibitor VAS2870 decreased the Nox4 mRNA expression in a concentration-dependent manner.

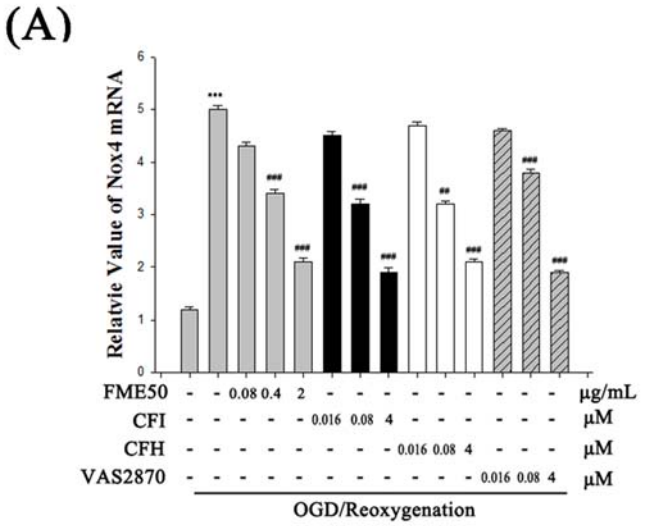

Fig. 6. The inhibitory effects of FME50, CFI, CFH or VAS2870 on the expression of Nox4 mRNA **(A)**. Nox4 mRNA expression was evaluated by RT-PCR assay, and Nox enzyme activity in SH-SY5Y cell was evaluated using lucigenin after treatment with different concentrations of FME (0.8 – 2 µg/ml), CFI, CFH or VAS2870 (0.8 – 2 µM) and exposure to OGD/R condition.

3.5. Inhibitory effect against OGD/R-induced down-regulation of miRNA-25, miRNA-92a, and miRNA-146a in SH-SY5Y cells

To evaluate the effect of FME50, CFI, and CFH on Nox4-targeting three miRNAs expression, we performed the qRT-PCR assay. The expression of miRNA-25, miRNA-92a, and miRNA-146a was decreased by OGD/R condition (Fig. 7). FME50, CFI, and CFH attenuated OGD/R-induced decrease of Nox4-targeting three miRNAs expression in SH-SY5Y cells. FME50 (2 μg/mL), CFI, and CFH (4 μM) almost restored to a normal level of Nox4-targeting three miRNAs expression (Fig. 7A – C). VAS2870 also restored OGD/R-induced three miRNAs expression in a concentration-dependent manner (Fig. 7A – C).

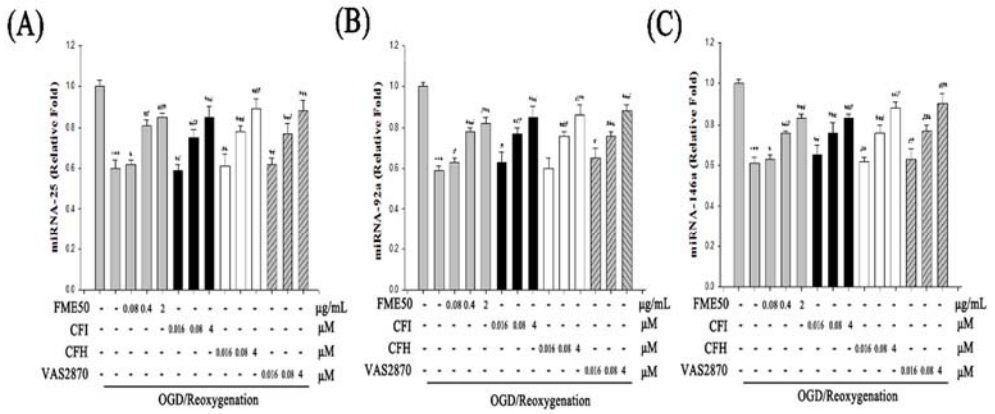

Fig. 7. Quantitative comparison of the miRNA-25, miRNA-92a, and miRNA-146a level in the OGD/R-induced condition in SH-SY5Y cells. The cells were treated with different concentrations of FME50 (0.08 – 2 μg/ml), CFI, CFH, or VAS2870 (0.16 – 4 μM) **(A-C)**. The results were expressed as fold change compared with the OGD/R condition. Data represent the mean ± SD of three independent experiments. ($^{\#}p<0.05$, $^{\#\#}p<0.01$ and $^{\#\#\#}p<0.001$ compared to the control group)

3.6. Inhibitory effect against OGD/R-induced Nox enzyme activity in SH-SY5Y cell

Based on the results of Nox4 mRNA expression, we examined the inhibitory effect of FME50, CFI, and CFH on Nox enzyme activity. The Nox enzyme activity was significantly increased in OGD/R-induced SH-SY5Y cells. However, FME50, CFI, and CFH inhibited OGD/R-induced Nox enzyme activity in a concentration-dependent manner with an IC_{50} values of 1.1 μg/mL, 2.7 μM, and 1.9μM, respectively (Fig. 8). Also, VAS2870 inhibited Nox enzyme activity with an IC_{50} values of 2.1 μM.

(A)

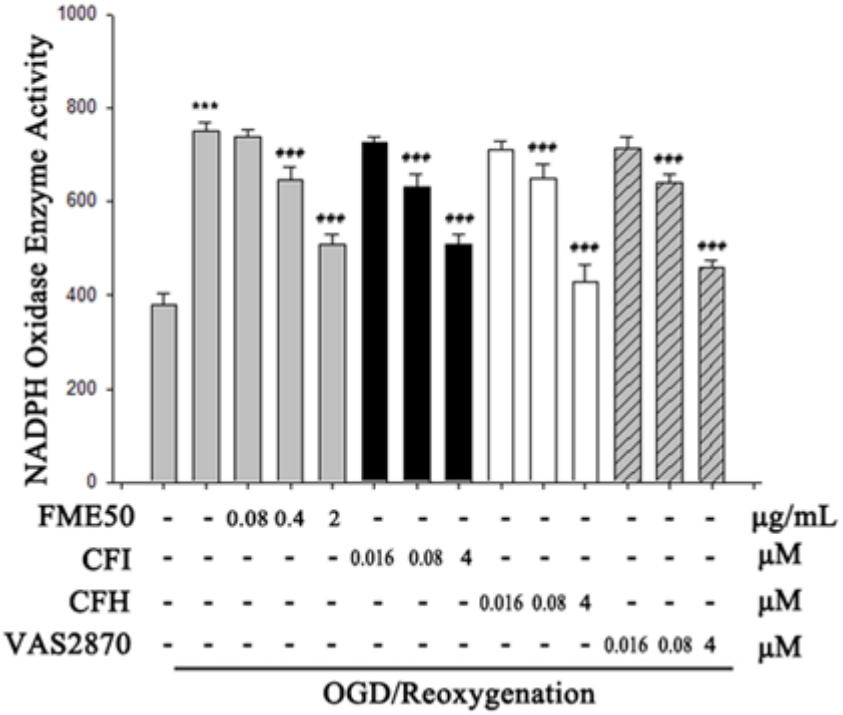

Fig. 8. The inhibitory effects of FME50, CFI, CFH or VAS2870 on the expression of Nox enzyme activity **(A)**. Nox4 mRNA expression was evaluated by RT-PCR assay, and Nox enzyme activity in SH-SY5Y cell was evaluated using lucigenin after treatment with different concentrations of FME50 (0.08 – 2 µg/ml), CFI, CFH or VAS2870 (0.016 – 4 µM) and exposure to OGD/R condition.

3.7. Inhibitory effect of FME50 on NADPH oxidase (NOX) enzyme activity in whole cell lysates

The inhibitory effect of FME50 and VAS2870 on NOX enzyme activity was measured using SH-SY5Y whole cell lysates. As shown in Fig. 9, NOX enzyme activity was inhibited FME50 or VAS2870 with an IC_{50} values of 5.6 μg/mL and 14.7 μM, respectively. The inhibitory potency of NOX enzyme by FME50 was 2.1-fold higher than VAS2870.

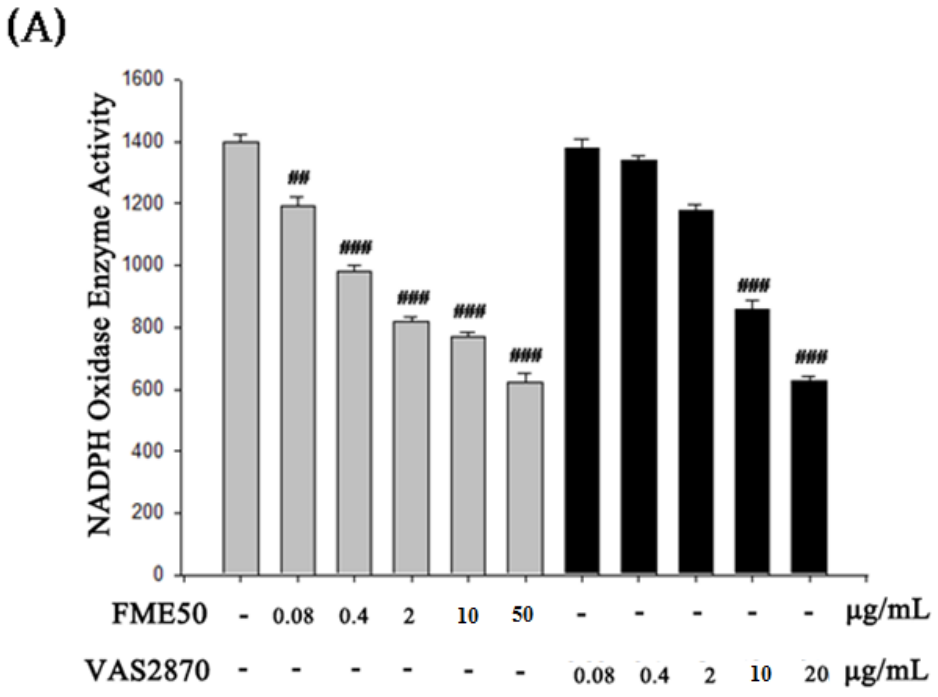

Fig. 9. The inhibitory effects of FME50 or VAS2870 on Nox enzyme activity **(A)**. Nox enzyme activity in SH-SY5Y cell was evaluated using lucigenin after treatment with different concentrations of FME50 (0.08 – 50 µg/ml), or VAS2870 (0.08 – 20 µM). Data represent the mean ± SD of three independent experiments. ($^{\#}p<0.05$, $^{\#\#}p<0.01$ and $^{\#\#\#}p<0.001$ compared to the control group)

3.8. Inhibitory effects against OGD/R-induced Nox4 mRNA expression

It was reported that miRNA-25, miRNA-92a, and miRNA-146a down-regulated Nox4 mRNA expression (Fu et al., 2010; Wang et al., 2014; Tsao et al., 2015). In correlated with previous study, Nox4-related three miRNAs mimic inhibited OGD/R-induced Nox4 mRNA expression (Fig. 10). However, three miRNAs inhibitor exacerbate OGD/R-induced increase of Nox4 mRNA expression (Fig. 10).

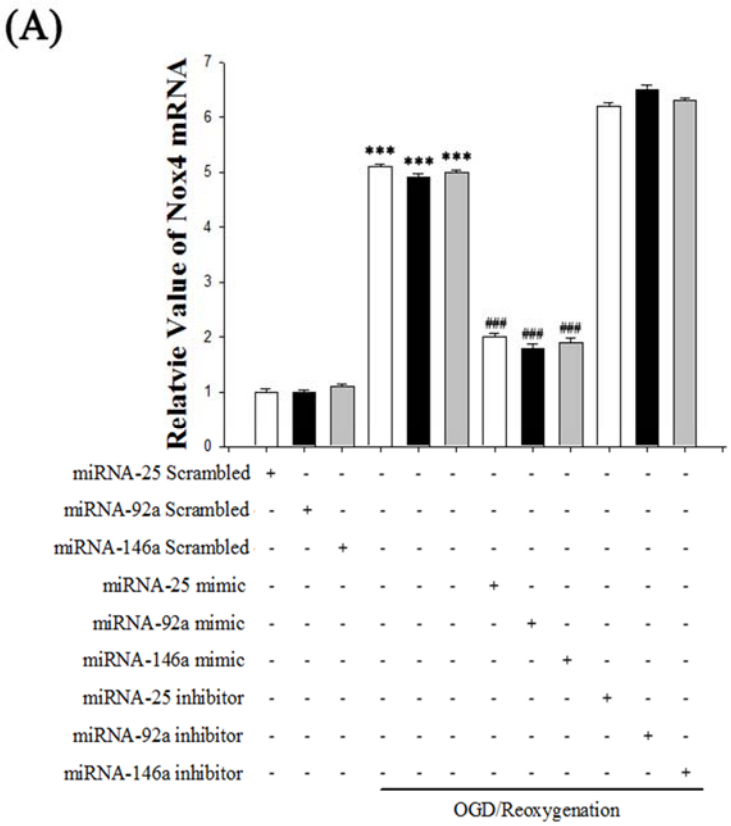

Fig. 10. Quantitative comparison of Nox4 mRNA level in OGD/R-induced in SH-SY5Y cell. The cells were transfected with 200nM of three different miRNAs scrambled, mimics and inhibitor **(A)** and exposed to OGD/R conditions Data represent the mean ± SD of three independent experiments. ($^{\#}p<0.05$, $^{\#\#}p<0.01$ and $^{\#\#\#}p<0.001$ versus control group)

3.9. Inhibitory effect against OGD/R-induced ASK1-JNK/p38 MAPK apoptotic signaling pathway

It has been reported that OGD/R condition induces excessive ROS accumulation by Nox4 activation. The excessive ROS generation induces apoptosis through phosphorylating ASK1-JNK/p38 MAPK factors which are the evidence of MAPK signal activation (Lai et al., 2007). In our results, OGD/R condition increased the Nox4 protein expression. Also, OGD/R increased phosphorylation of ASK-1, JNK1, and p38 protein and cleavage of caspase3 (Fig. 11). FME50, CFI, and CFH attenuated OGD/R-induced increase of Nox4 protein and increase of phosphorylated ASK-1, JNK1, and p38 protein in a concentration-dependent manner (Fig. 11A - C). In addition, FME50, CFI and CFH inhibited the cleavage of caspase-3 (Fig. 11A - C). As shown in Fig. 10D, VAS2870 restored OGD/R-induced changed protein expression of Nox4, p-ASK1, p-JNK1, p-p38, and cleaved caspase3 to normal in a concentration-dependent manner.

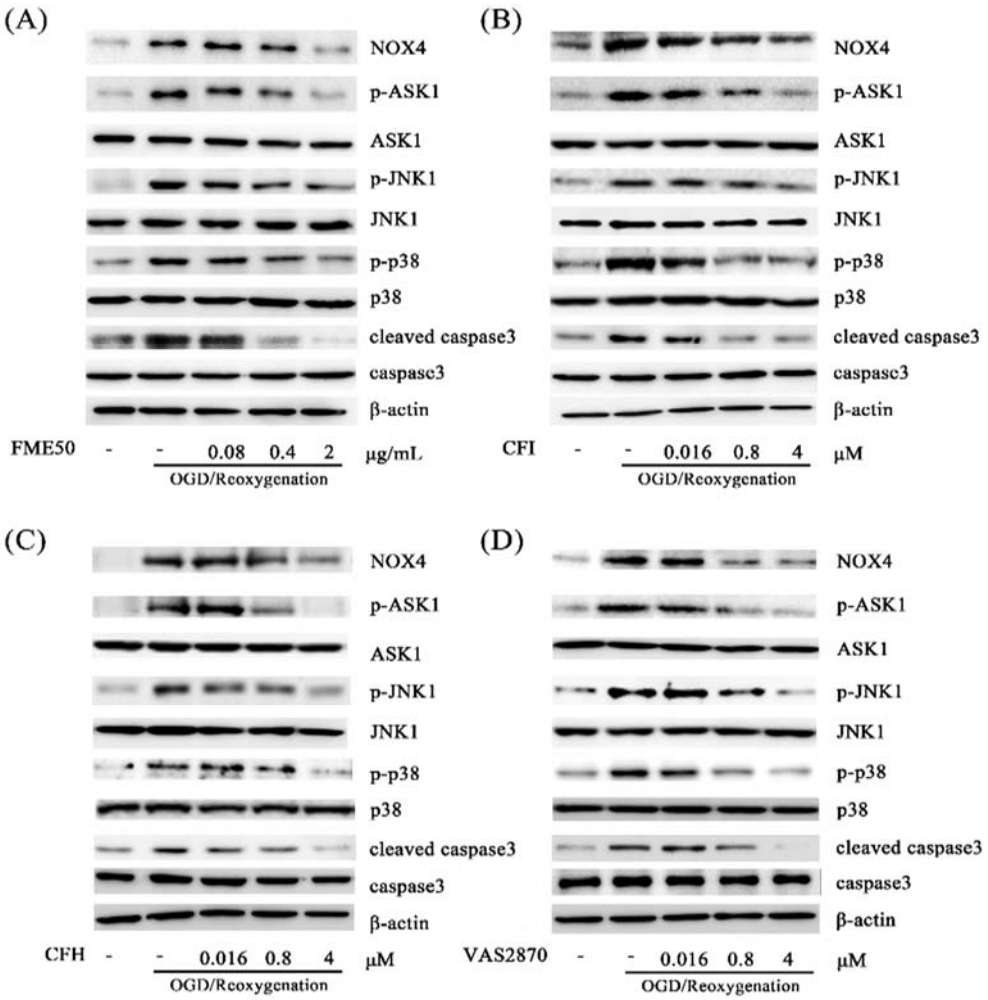

Fig. 11. Inhibitory effects of FME50, CFI, CFH or VAS2870 on the expression levels of Nox4, p-ASK1, ASK1, p-JNK1, JNK1, p-p38, p38 and β-actin were evaluated by western blot analysis. The cells were treated with different concentrations of FME50 (0.08 – 2 μg/ml) **(A)**, CFI, CFH, or VAS2870 (0.016

– 4 μM) **(B-D)** and exposed to OGD/R conditions**.** Data represent the mean ± SD of three independent experiments. ($^{***}p<0.001$ compared to the control group, $^{\#}p<0.05$, $^{\#\#}p<0.01$ and $^{\#\#\#}p<0.001$ compared to the OGD/R-induced group).

3.10. Protective effect of carnosine against OGD/R-induced cytotoxicity in SH-SY5Y cells

The protective effect of carnosine against OGD/R-induced neuronal cell death was evaluated by MTT assay within nontoxic concentration ranges. As shown in Fig. 11A, the cell viability of OGD/R-induced group was decreased compared to the normal control group. In contrast, carnosine (0.08, 0.4, and 2 μM) protected against OGD/R-induced cell death in a concentration-dependent manner, with an EC_{50} of 13.4 μM.

3.11. Inhibitory effect of carnosine against OGD/R-induced intracellular ROS generation in SH-SY5Y cells

Intracellular ROS was measured by DCFH-DA. DCFH-DA is diffuses through the cell membrane and is deacetylated by cellular esterase. Through this process, DCFH-DA makes its non-fluorescent form, dichlorodihydrofluorescein (DCFH). DCFH can be rapidly oxidized by intracellular ROS and converts to the highly fluorescent form, dichlorofluorescein (DCF) (Ratner et al., 1987). As shown in Fig. 11B, the OGD/R-induced cells exhibited strong DCF fluorescence intensity compared to normal control group. The extent of OGD/R-induced ROS production was decreased by carnosine (0.08 - 2 μM) in a concentration-dependent manner.

(A)

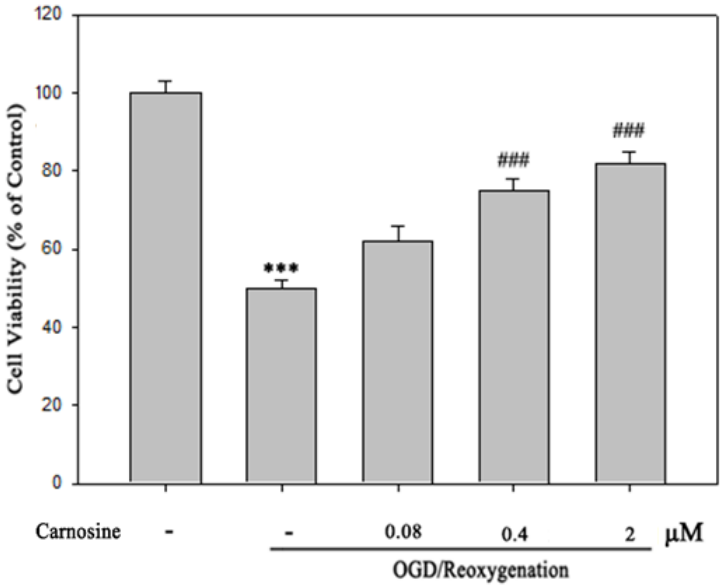

Fig. 12. The effect of carnosine on OGD/R-induced cell death in SH-SY5Y cells was measured by an MTT reduction assay. The cells were treated with different concentrations of carnosine (0.08 – 2 μg/ml) exposed to OGD/R conditions **(A).**

(B)

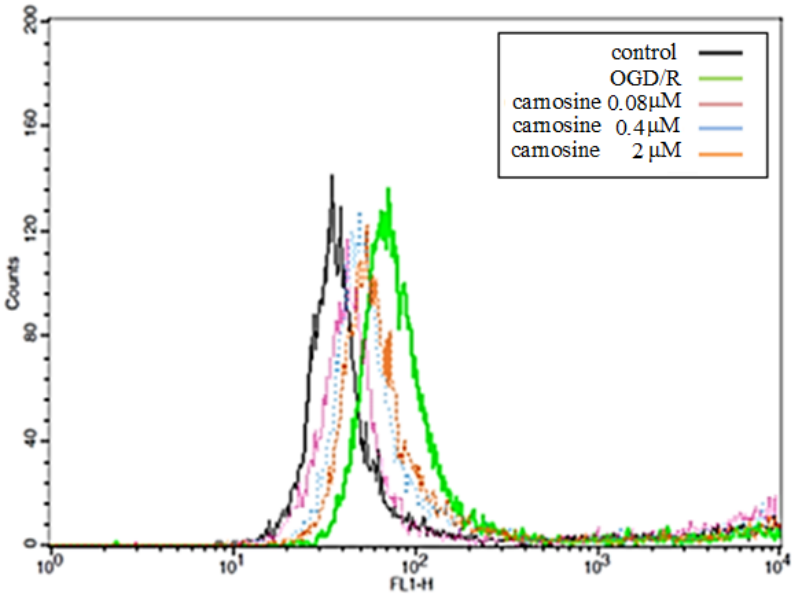

Fig. 13. The effects of carnosine on OGD/R-induced intracellular ROS generation in SH-SY5Y cells are illustrated by DCFH-DA staining. The cells were treated with different concentrations of carnosine (0.08 – 2 μM) **(B)** and exposed to OGD/R conditions. Data represent the mean ± SD of three independent experiments. ($^{***}p<0.001$ compared to the control group, $^{\#}p<0.05$, $^{\#\#}p<0.01$ and $^{\#\#\#}p<0.001$ compared to the OGD/R-induced group).

3.12. Protective effect against MCAO/R-induced brain infarct

The neuroprotective effect of FME50 was evaluated in MCAO/R-induced ischemic rats by measuring the reduction ratio of infarct volume (Fig. 12). As shown in Fig. 12, the dose of administration was used within non-toxic ranges and the infarct volume was estimated. The infarct volume of FME50-treated groups (25, 50, and 100 mg/kg) were decreased to 33.0 ± 1.3%, 24.0 ± 4.2%, and 18.0 ± 3.6%, respectively, whereas vehicle-treated group was 47.9 ± 1.5% (Fig. 12). In subsequent experiments, carnosine, reported that it has neuroprotective effect on the early stage of focal ischemia, was used as a control compound. The infarct volume of carnosine-treated groups (25, 50, and 75 mg/kg) was reduced to 35.6 ± 4.2%, 22.0 ± 3.5%, and 13.6 ± 5.2%, respectively (Fig. 12). In our results showed that FME50 provided a potent protective effect of brain infarct in MCAO/R-induced ischemic rats.

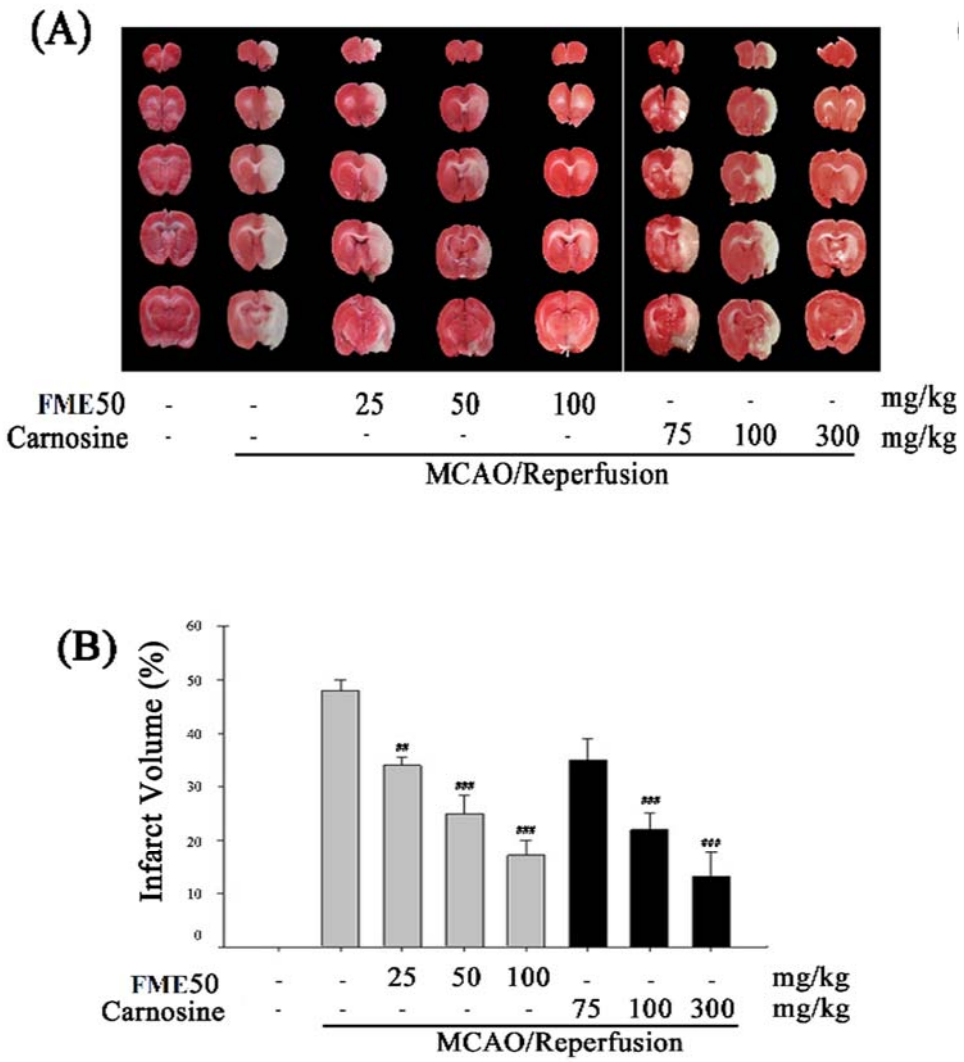

Fig. 14. The effects of FME50 on the MCAO/R-induced cerebral infarct volume in the rat brain.

Five consecutive, 2-mm-thick slices were stained with TTC to visualize the MCAO/R-induced infarct volume in the rat brain. Representative images of rat brain slices are shown from each group treated with FME50 (25 - 100 mg/kg) or carnosine (75 – 300 mg/kg). Data represent the mean ± SD of six independent experiments (A). The infarct volume ratio in each group was quantified using ImageJ software, and the quantitative value was shown as a histogram bar with the SD value (B).

3.13. Inhibitory effect against MCAO/R-induced reciprocal down-regulation of miRNA-25, miRNA-92a, and miRNA-146a

Nox4 plays a major role in the pathological signaling pathway of cerebral ischemia. MiRNA-25, miRNA-92a, and miRNA-146a is one of regulators to protect neuronal cell death by inhibiting Nox4 mRNA expression (Fu et al., 2010; Wang et al., 2014; Tsao et al., 2015). The Nox4-targeting three miRNAs were significantly decreased in MCAO/R-induced group (Fig. 13). Additionally, carnosine-treated group (75-300 mg/kg) attenuated the increase of Nox4 protein and decreased of three miRNAs expression in MCAO/R-induced brain injury (Fig. 13).

(A)

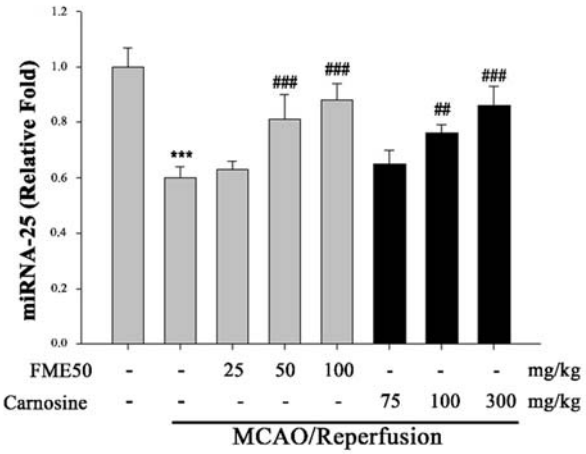
miRNA-25 (Relative Fold)
1.2
1.0
0.8
0.6
0.4
0.2
0.0
***
###
###
##
###
FME50 - - 25 50 100 - - - mg/kg
Carnosine - - - - - 75 100 300 mg/kg
MCAO/Reperfusion

(B)

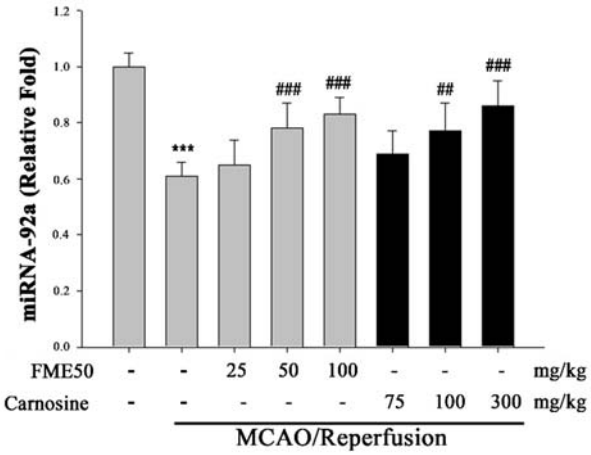
miRNA-92a (Relative Fold)
1.2
1.0
0.8
0.6
0.4
0.2
0.0
***
###
###
##
###
FME50 - - 25 50 100 - - - mg/kg
Carnosine - - - - - 75 100 300 mg/kg
MCAO/Reperfusion

(C)

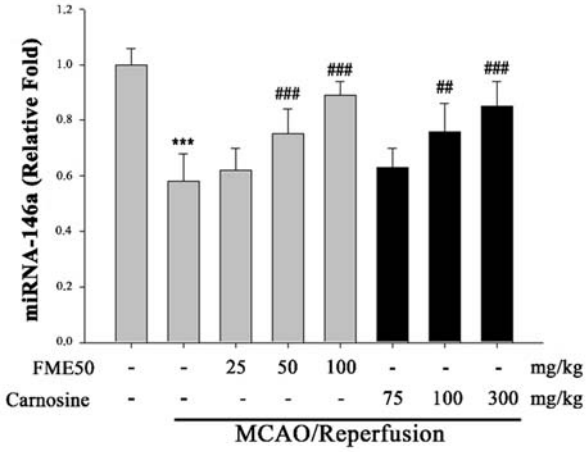

Fig. 15. Quantitative comparison of miRNA-25, miRNA-92a, and miRNA-146a levels in MCAO/R-induced rats. The rats were treated with different concentrations of FME50 (25 - 100 mg/kg) or carnosine (75 – 300 mg/kg) **(A-C)** and exposed to MCAO/R conditions. Data represent the mean ± SD of three independent experiments. ($^{\#}p<0.05$, $^{\#\#}p<0.01$ and $^{\#\#\#}p<0.001$ compared to the control group)

3.14. Inhibitory effect against MCAO/R-induced reciprocal up-regulation of Nox4 mRNA

The inhibitory effect of FME50 against MCAO/R–induced Nox4 mRNA expression was measured by RT-PCR analysis. It has been reported that the Nox family plays a crucial role in the pathological signaling pathway induced by cerebral ischemia. In particular, Nox4 is expressed in neuronal tissues and plays a critical role in the production of ROS in brain tissue (Bedard and Krause, 2007). The Nox4 mRNAs were significantly decreased in MCAO/R-induced group compared to the sham control group (Fig. 14). Additionally, carnosine-treated group (75-300 mg/kg) attenuated the decrease of Nox4 mRNA MCAO/R-induced brain injury (Fig. 14).

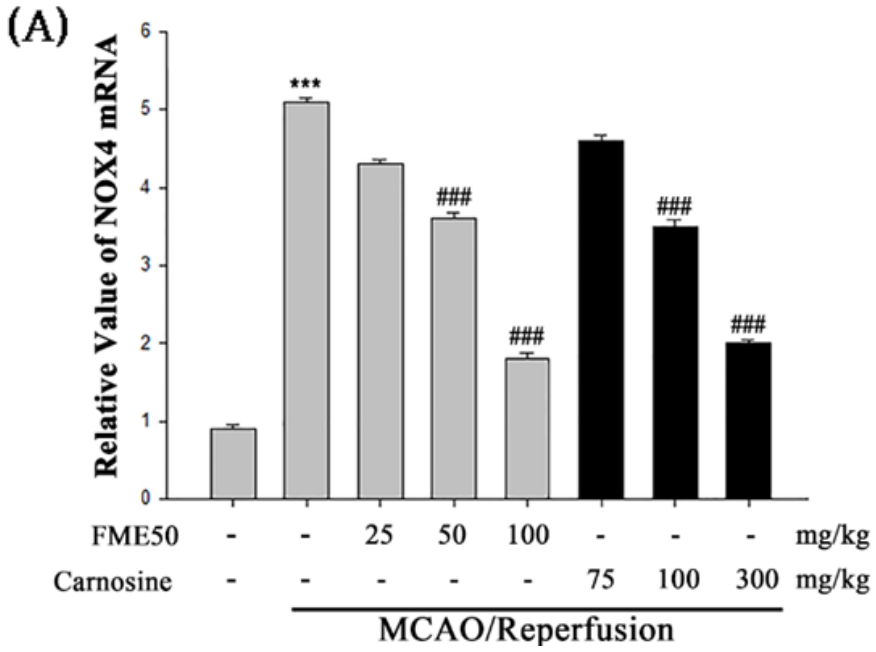

Fig. 16. The inhibitory effects of FME50 or carnosine on the expression of Nox4 mRNA. Nox4 mRNA expression of rats treated with FME50 (25 - 100 mg/kg) or carnosine (75 – 300 mg/kg) and exposed to MCAO/R conditions **(A).** Data represent the mean ± SD of three independent experiments. ($^{\#}p<0.05$, $^{\#\#}p<0.01$ and $^{\#\#\#}p<0.001$ compared to the control group)

3.15. Inhibitory effect against MCAO/R-induced ASK1-JNK/p38 MAPK apoptotic signaling pathway

The activation of MAPK pathway by excessive ROS induces apoptosis (Choi et al., 2009). As shown in Fig. 15, Nox4 protein expression was significantly increased in MCAO/R-induced group compared to the sham control group. However, FME50-treated groups (25, 50 and 100 mg/kg) and carnosine-treated groups (75, 100, and 300 mg/kg) decreased Nox4 protein expression. The MCAO/R-induced brain injury caused the activation of ASK1-JNK/p38 MAPK apoptotic signaling pathway by phosphorylating ASK1, JNK1, and p-p38. Also, the cleavage of caspase-3 was increased after MCAO/R-induced brain injury. However, FME50-treated groups (25, 50 and 100 mg/kg) inhibited the phosphorylation of ASK1, JNK1, and p38 and cleavage of caspase-3 (Fig. 15A). Carnosine-treated groups (75, 100, and 300 mg/kg) also inhibited activation of MAPK signal cascades (Fig. 15B). Hence, FME50 and carnosine protected MCAO/R-induced apoptosis via the inhibition of MAPK apoptotic signaling pathway.

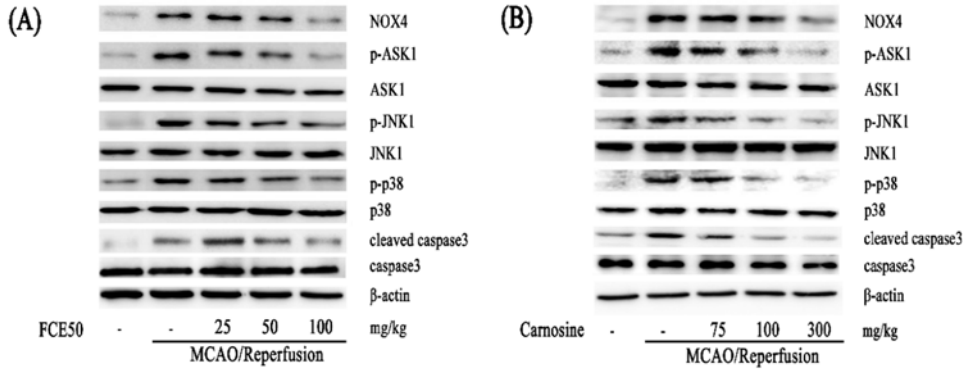

Fig. 17. The effect of FME50 on protein expression in MCAO/R-induced rat brain injury. The protein expression levels of Nox4, p-ASK1, ASK1, p-JNK1, JNK1, p-p38, p38 and β-actin in ischemic cerebrum of rats treated with FME50 (25 - 100 mg/kg) **(A)** or carnosine FME50 (75 - 300 mg/kg) were evaluated by western blots. Representative images from six independent experiments are shown.

3.16. Inhibitory effect against OGD/R-induced reciprocal up-regulation of Ago1 and Ago2 mRNA

MicroRNAs associate with protein of the Ago family gorming ribonucleoprotien complexes (RISCs) that regulate gene expression at transcriptional or post-transcriptional level. miRNAs are derived from endogenously encoded genes, some of which are found in cluster, in inter or intragenic regions of protein coding genes. FME50-treated group (0.08 – 2 μg/mL) markedly inhibited OGD/R-induced decrease of Ago1 and Ago2 mRNA expression (Fig. 16 and Fig. 17). The results were correlated with the results of *in vitro* model. Additionally, CFI and CFH-treated group (0.016 – 4 μM) attenuated the decrease of Ago1 and Ago2 mRNA expression in OGD/R-induced brain injury (Fig. 16 and Fig. 17).

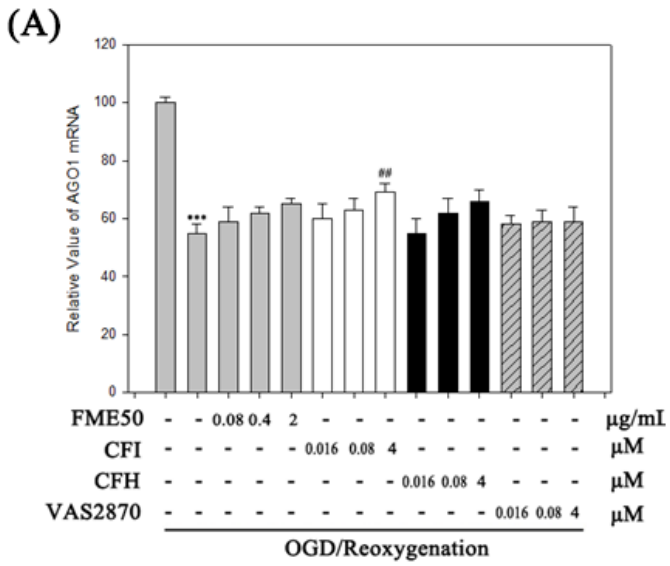

Fig. 18. Quantitative comparison of Ago1 mRNA level in OGD/R-induced in SH-SY5Y cell. Ago1 mRNA expression was evaluated by RT-PCR assay. The cells were treated with different concentrations of FME50 (0.08 – 2 µM) or CFI, CFH, VAS2870 (0.016 – 4 µM) and exposed to OGD/R conditions Data represent the mean ± SD of three independent experiments. ($^{\#}p<0.05$, $^{\#\#}p<0.01$ and $^{\#\#\#}p<0.001$ versus control group)

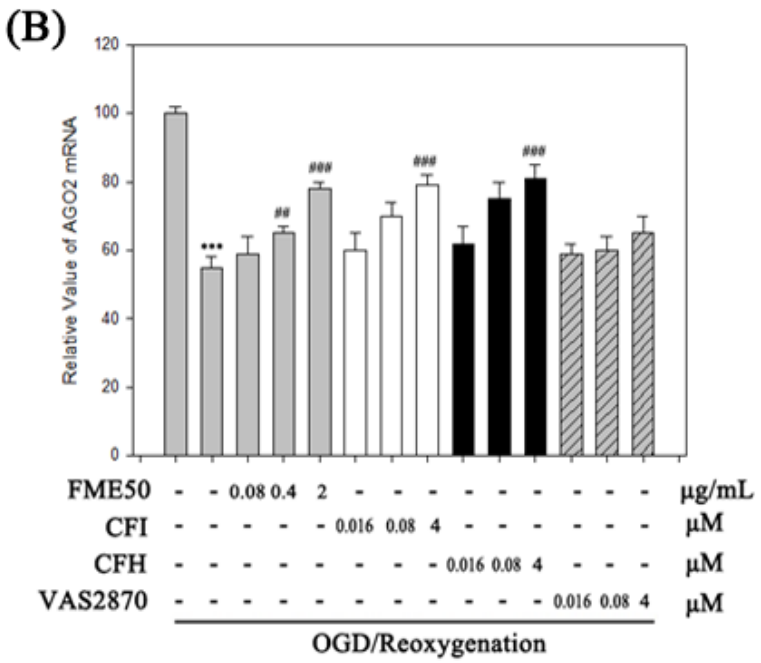

Fig. 19. Quantitative comparison of Ago2 mRNA level in OGD/R-induced in SH-SY5Y cell. Ago2 mRNA expression was evaluated by RT-PCR assay. The cells were treated with different concentrations of FME50 (0.08 – 2 µM) or CFI, CFH, VAS2870 (0.016 – 4 µM) and exposed to OGD/R conditions Data represent the mean ± SD of three independent experiments. ($^{\#}p<0.05$, $^{\#\#}p<0.01$ and $^{\#\#\#}p<0.001$ versus control group)

4. Discussion

Ischemic stroke is a leading cause of death and long-lasting disability, but therapeutic options remain limited and not clearly verified. Recent research suggested that miRNAs play crucial role in pathogenesis of cerebral ischemia brain injury (Junn and Mouradian, 2012). MicroRNAs are targeting a single gene by transcriptional control and cellular redox regulation(Ouyang et al., 2015). After maturation, microRNAs are single stranded RNA molecules to derived long hairpin-precursor known as pre-miRNA. The pre-miRNA is transported to cytoplasm and microRNAs loaded onto the RISC complex can bind a direct target of mRNA 3'-untranslated region (3'-UTR). The binding of miRNAs leads to regulate the mRNA expression of target proteins (Lancon et al., 2013). A recent study reported that miRNA-25, miRNA-92a, and miRNA-146a acted as a critical regulator of Nox4 in neuronal cell (Jeyaseelan et al., 2008). In correlated with previous research results, Nox4-related three miRNAs contributed to the regulation of Nox4 expression in SH-SY5Y cells. Nox4 is a member of the NADPH oxidase family and activation of Nox4 increases intracellular ROS (Siuda et al., 2012). The excessive ROS generation induces cellular stress and damages organelles. Also, it induces

apoptosis via activation of ASK1-JNK/p38 MAPK signaling pathway (Mochizuki et al., 2006). The redox sensor proteins thioredoxin (Trx) inhibit the kinase activity of ASK1 through binding to ASK1. Once eexcessive ROS was generated, Trx is unable to associate with ASK1. Hence, the activated ASK-1 induces the phosphorylation of JNK1 and p38 (Mantzaris et al., 2016). Finally, p-p38 induces activation of caspase-3 by making cleaved form of caspase-3, which is the key factor involved in the apoptotic process in neuronal cell (Ghosh et al., 2011). Thus, the inhibition of Nox4 expression and Nox enzyme activity through the up-regulation of Nox4-related three miRNAs is one of primary mechanisms regulating excessive ROS generation, and ASK1-JNK/p38 MAPK signal mediated apoptosis.

In the present study, OGD/R-induced ROS generation and neuronal cell death was attenuated in a concentration-dependent manner when cells were treated with different concentrations of FME50, CFI, and CFH. To investigate how FME50, CFI, and CFH inhibited OGD/R-induced ROS generation, we evaluated the effects of them on the Nox4 protein expression and Nox enzyme activity. Recent study demonstrated that Nox in neurons produced intracellular ROS under ischemic conditions (Vallet et al., 2005). In our results, Nox4 protein and enzyme activity were increased in OGD/R model, whereas Nox4

protein and enzyme activity were markedly reduced by FME50, CFI, and CFH treatment. Also, VAS2870, known as Nox inhibitor, attenuated OGD/R-induced Nox4 protein and enzyme activity and OGD/R-induced ROS generation. The results demonstrated that Nox4 inhibition reduced OGD/R-induced excessive ROS generation in SH-SY5Y cells. Additionally, FME50, CFI, and CFH protected OGD/R-induced intracellular ROS generation and cell death via inhibition of Nox4 protein and enzyme. To elucidate the underlying mechanism of Nox4 inhibitory effect, we examined the miRNAs which are known as a regulator of Nox4. It was previously demonstrated that miRNA-25, miRNA-92a, and miRNA-146a inhibited Nox4 mRNA expression (Fu et al., 2010; Wang et al., 2014; Tsao et al., 2015). To confirm the effect of Nox4-targeting miRNAs on Nox4 expression, we examined the effects of mimics and inhibitors of Nox4-targeting three miRNAs on OGD/R-induced Nox4 mRNA expression. In correlated with the results of previous studies, miRNA mimic transfection significantly inhibited OGD/R-induced Nox4 mRNA expression. However, miRNA inhibitors slightly increased OGD/R-induced Nox4 mRNA expression. We evaluated the effects of FME50, CFI, and CFH on miRNA-25, miRNA-92a, and miRNA-146a expression. FME50, CFI, and CFH significantly increased the all of Nox4-targeting three miRNAs expression in a concentration-dependent manner. FME50, CFI, and

CFH showed no selectivity on three miRNAs. The results can be interpreted that argonaute, up-stream factor of miRNAs, will be regulated by FME50, CFI, and CFH and argonaute regulated all of three miRNAs. To reveal this hypothesis, further study should be conducted in the near future. The results suggested that FME50, CFI, and CFH inhibited OGD/R-induced Nox4 activation by up-regulation of Nox4-targeting three miRNAs and ultimately protected OGD/R-induced excessive ROS generation and neuronal cell death in SH-SY5Y cell. A growing body of evidence suggested that ROS-mediated ASK1 activation plays an important role in OGD/R-induced apoptosis in neurodegenerative diseases and several studies suggested that ASK1-targeted drugs expected to mitigate neurodegenerative diseases (Ichijot et al., 2009). The OGD/R-induced cell exhibited the significant increase of p-ASK1, p-JNK1, p-p38, and cleaved caspase3 protein expression. This results show that OGD/R-induced ROS activates ASK1-JNK3/p38 MAPK apoptotic signal and induces neuronal cell death (Mantzaris et al., 2016; Ghosh et al., 2011). In our results, FME50, CFI, and CFH suppressed OGD/R-induced activation of MAPK apoptotic signal. Also, VAS2870 inhibited MAPK apoptotic signal activation. This result suggested that the protective effect of FME50, CFI, and CFH on OGD/R-induced ROS suppressed the activation of MAPK apoptotic signal and protected neuronal cell death.

Based on the results of *in vitro* model, we conducted the experiment about FME50 using MCAO/R *in vivo* model of cerebral ischemia. In correlated with the result of *in vitro* model, FME50 elicited its neuroprotective effects against MCAO/R-induced brain infarct. Also, carnosine which was reported that it has neuroprotective effects in the early stage of focal ischemia and protects brain tissues and mitochondrial dysfunction from oxidative brain damage (Baek et al., 2014; Park et al., 2014) was used as a positive control compound and it exhibited protective effect with a dose dependent manner. The results showed that FME50 provided more potent neuroprotective effect against MCAO/R-induced brain infarct than carnosine. The previous study demonstrated that excessive ROS is generated by Nox4 after MCAO/R-induced stroke models in mice (Nishimura et al., 2016). On the basis of the results about Nox4 protein expression and Nox4-targeting miRNA-25, miRNA-92a, and miRNA-146a expression in *in vitro* model, we evaluated the effects of FME50 and carnosine on Nox4 mRNA, protein expression and Nox4-targeting three miRNAs expression in *in vivo* model. The Nox4 mRNA, protein expression was increased in the MCAO/R-induced brain, whereas FME50-treated group and carnosine-treated group attenuated the increase of MCAO/R-induced Nox4 mRNA, protein expression. Also, Nox4-targeting three miRNAs was decreased in the MCAO/R-induced brain. However,

FME50-treated group and carnosine-treated group restored the MCAO/R-induced miRNAs expression to normal state. This result was correlated with that of *in vitro* model. Additionally, we investigated the ASK1-JNK1/p38 MAPK signal cascade. It was reported that MCAO/R condition exacerbates ROS generation in neuron (Chouchani et al., 2014). Because of excessive ROS, MAPK apoptotic signal is activated in MCAO/R-induced brain. In our results, phosphorylation of AKS1, JNK1, and p38 and cleavage of caspase3 were increased in MCAO/R-induced brain. FME50-treated group and carnosine-treated group inhibited MCAO/R-induced activation of MAPK signal cascade and protected brain infarct. Consistent with the result of in vitro model, FME50 protected MCAO/R-induced brain infarct through MAPK apoptotic signal cascade.

5. Conclusion

This study demonstrated the neuroprotective effects of FME50, CFI, and CFH on *in vitro* and *in vivo* models of cerebral ischemia. FME50 protected OGD/R-induced neuronal cell death and excessive ROS generation in *in vitro* model. Also, FME50 protected MCAO/R-induced brain infarct in *in vivo* model. FME50 significantly suppressed Nox4 mRNA, protein expression by regulating Nox4-targetomg miRNA-25, miRNA-92a, and miRNA-146a and it attenuated the ASK1-JNK/p38 MAPK apoptotic signal pathway. Additionally, CFI and CFH, one of compounds from FME50, showed protective effect against OGD/R-induced ROS generation and cell death. CFI and CFH also exhibited the regulatory effects on Nox4, Nox4-targeting miRNAs, and MAPK apoptotic signal pathway. Taken together, we suggest that FME50, CFI, and CFH might be promising candidates for the therapy of cerebral ischemia.

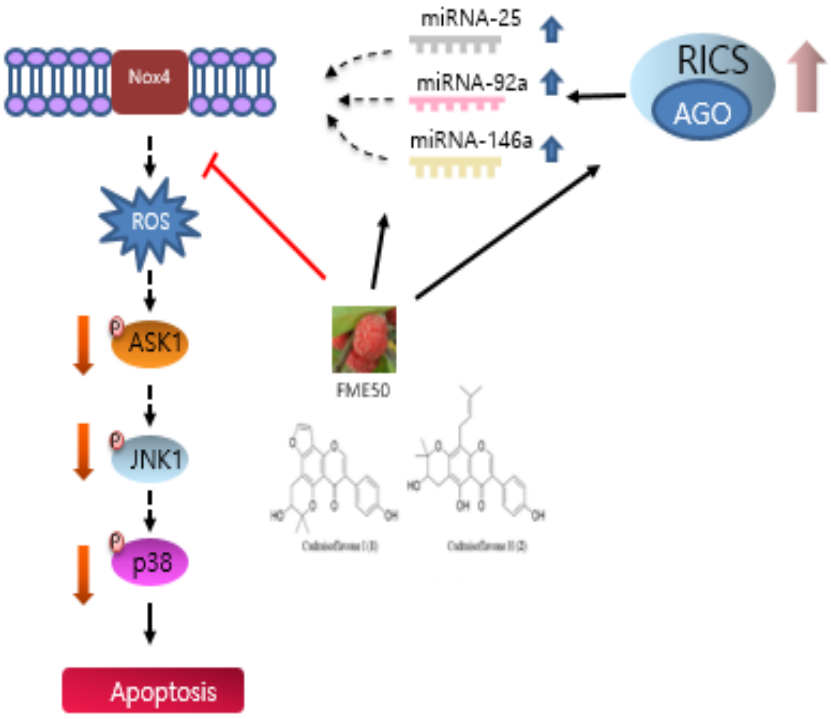

Fig. 20. A scheme of the inhibitory effects of FME50, CFI, and CFH on Nox4 mRNA targeting miRNAs signaling in SH-SY5Y cells. FME50, CFI, and CFH inhibited ASK1-JNK/p38 MAPK apoptotic signal pathway. The Nox4-targetomg miRNA-25, miRNA-92a, and miRNA-146a significantly upregulated by FME50, CFI, and CFH. In addition, FME50, CFI, and CFH increasing the Ago1 and Ago2 mRNA expression.

References

Adlakha, YK, Saini, N. 2014. Brain microRNAs and insights into biological functions and therapeutic potential of brain enriched miRNA-128. *Mol Cancer* **13**.

Baek, SH, Noh, AR, Kim, KA, Akram, M, Shin, YJ, Kim, ES, et al. 2014. Modulation of Mitochondrial Function and Autophagy Mediates Carnosine Neuroprotection Against Ischemic Brain Damage. *Stroke* **45**(8): 2438-2443.

Bedard, K, Krause, KH. 2007. The NOX family of ROS-generating NADPH oxidases: physiology and pathophysiology. *Physiological reviews* **87**(1): 245-313.

Chan, PH. 2001. Reactive oxygen radicals in signaling and damage in the ischemic brain. *Journal of cerebral blood flow and metabolism : official journal of the International Society of Cerebral Blood Flow and Metabolism* **21**(1): 2-14.

Cho, EY, Lee, SJ, Nam, KW, Shin, J, Oh, KB, Kim, KH, et al. 2010. Amelioration of oxygen and glucose deprivation-induced neuronal death by chloroform fraction of bay leaves (Laurus nobilis). *Bioscience, biotechnology, and biochemistry* **74**(10): 2029-2035.

Choi, JR, Heo, H, Lang, Y, Shin, KS, Kang, SJ. 2009. Apoptosis signal-regulating kinase 1 regulates the expression of caspase-11. *Febs Lett* **583**(18): 3016-3020.

Chouchani, ET, Pell, VR, Gaude, E, Aksentijevic, D, Sundier, SY, Robb, EL, et al. 2014. Ischaemic accumulation of succinate controls reperfusion injury through mitochondrial ROS. *Nature* **515**(7527): 431-435.

Farago, N, Kocsis, GF, Feher, LZ, Csont, T, Hackler, L, Jr., Varga-Orvos, Z, et al. 2008. Gene and protein expression changes in response to normoxic perfusion in mouse hearts. *Journal of pharmacological and toxicological methods* **57**(2): 145-154.

Fu, YB, Zhang, Y, Wang, ZY, Wang, LL, Wei, XB, Zhang, B, et al. 2010. Regulation of NADPH Oxidase Activity Is Associated with miRNA-

25-Mediated NOX4 Expression in Experimental Diabetic Nephropathy. *Am J Nephrol* **32**(6): 581-589.

Ganora, L. 2009. Herbal constituents: Foundations of phytochemistry. *Lisa Ganora, Louisville, CO*.

Ghaffari, H, Venkataramana, M, Ghassam, BJ, Nayaka, SC, Nataraju, A, Geetha, NP, et al. 2014a. Rosmarinic acid mediated neuroprotective effects against H2O2-induced neuronal cell damage in N2A cells. *Life Sci* **113**(1-2): 7-13.

Ghaffari, H, Venkataramana, M, Jalali Ghassam, B, Chandra Nayaka, S, Nataraju, A, Geetha, NP, et al. 2014b. Rosmarinic acid mediated neuroprotective effects against H2O2-induced neuronal cell damage in N2A cells. *Life Sci* **113**(1-2): 7-13.

Ghosh, J, Das, J, Manna, P, Sil, PC. 2011. The protective role of arjunolic acid against doxorubicin induced intracellular ROS dependent JNK-p38 and p53-mediated cardiac apoptosis. *Biomaterials* **32**(21): 4857-4866.

Ham, A, Kim, DW, Kim, KH, Lee, SJ, Oh, KB, Shin, J, et al. 2013. Reynosin protects against neuronal toxicity in dopamine-induced SH-SY5Y cells and 6-hydroxydopamine-lesioned rats as models of Parkinson's disease: Reciprocal up-regulation of E6-AP and down-regulation of alpha-synuclein. *Brain Res* **1524**: 54-61.

Han, XH, Hong, SS, Jin, Q, Li, D, Kim, HK, Lee, J, et al. 2009. Prenylated and benzylated flavonoids from the fruits of Cudrania tricuspidata. *Journal of natural products* **72**(1): 164-167.

Hiep, NT, Kwon, J, Kim, DW, Hwang, BY, Lee, HJ, Mar, W, et al. 2015a. Isoflavones with neuroprotective activities from fruits of Cudrania tricuspidata. *Phytochemistry* **111**: 141-148.

Hiep, NT, Kwon, J, Kim, DW, Hwang, BY, Lee, HJ, Mar, W, et al. 2015b. Isoflavones with neuroprotective activities from fruits of Cudrania tricuspidata. *Phytochemistry* **111**: 141-148.

Hiney, JK, Srivastava, VK, Les Dees, W. 2010. Insulin-like growth factor-1 stimulation of hypothalamic KiSS-1 gene expression is mediated by

Akt: effect of alcohol. *Neuroscience* **166**(2): 625-632.

Hong, S, Kwon, J, Kim, DW, Lee, HJ, Lee, D, Mar, W. 2017. Mulberrofuran G Protects Ischemic Injury-induced Cell Death via Inhibition of NOX4-mediated ROS Generation and ER Stress. *Phytotherapy research : PTR* **31**(2): 321-329.

Hwang, HW, Mendell, JT. 2006. MicroRNAs in cell proliferation, cell death, and tumorigenesis. *Brit J Cancer* **94**(6): 776-780.

Ichijo, H, Fujisawa, T, Takeda, K. 2007. ASK family proteins in stress response and disease. *Mol Biotechnol* **37**(1): 13-18.

Ichijot, H, Homma, K, Katagiri, K, Nishitoh, H. 2009. Targeting ASK1 in ER stress-related neurodegenerative diseases. *Expert Opin Ther Tar* **13**(6): 653-664.

Irving, EA, Bamford, M. 2002. Role of mitogen- and stress-activated kinases in ischemic injury. *J Cerebr Blood F Met* **22**(6): 631-647.

Jeong, CH, Choi, GN, Kim, JH, Kwak, JH, Jeong, HR, Kim, DO, et al. 2010. Protective Effects of Aqueous Extract from Cudrania tricuspidata on Oxidative Stress-induced Neurotoxicity. *Food Science and Biotechnology* **19**(4): 1113-1117.

Jeong, JY, Jo, YH, Lee, KY, Do, SG, Hwang, BY, Lee, MK. 2014. Optimization of pancreatic lipase inhibition by Cudrania tricuspidata fruits using response surface methodology. *Bioorganic & medicinal chemistry letters* **24**(10): 2329-2333.

Jeyaseelan, K, Lim, KY, Armugam, A. 2008. MicroRNA expression in the blood and brain of rats subjected to transient focal ischemia by middle cerebral artery occlusion. *Stroke* **39**(3): 959-966.

Johnson, GL, Lapadat, R. 2002. Mitogen-activated protein kinase pathways mediated by ERK, JNK, and p38 protein kinases. *Science* **298**(5600): 1911-1912.

Jones, CG, Hare, JD, Compton, SJ. 1989. Measuring Plant Protein with the Bradford Assay .1. Evaluation and Standard Method. *J Chem Ecol*

15(3): 979-992.

Junn, E, Mouradian, MM. 2012. MicroRNAs in neurodegenerative diseases and their therapeutic potential. *Pharmacol Therapeut* **133**(2): 142-150.

K., SHMRM. 2011. The Nox Family of NADPH Oxidases that Deliberately Produce Reactive Oxygen Species. *Free Radical Biology in Digestive Diseases* **29**: 23-34.

Kang, DG, Hur, TY, Lee, GM, Oh, H, Kwon, TO, Sohn, EJ, et al. 2002. Effects of Cudrania tricuspidata water extract on blood pressure and renal functions in NO-dependent hypertension. *Life Sci* **70**(22): 2599-2609.

Kim, D-W, Kwon, J, Sim, SJ, Lee, D, Mar, W. 2017. Orobol derivatives and extracts from Cudrania tricuspidata fruits protect against 6-hydroxydomamine-induced neuronal cell death by enhancing proteasome activity and the ubiquitin/proteasome-dependent degradation of α-synuclein and synphilin-1. *Journal of Functional Foods* **29**: 104-114.

Kim, DW, Lee, KT, Kwon, J, Lee, HJ, Lee, D, Mar, W. 2015. Neuroprotection against 6-OHDA-induced oxidative stress and apoptosis in SH-SY5Y cells by 5,7-Dihydroxychromone: Activation of the Nrf2/ARE pathway. *Life Sci* **130**: 25-30.

Kim, JY, Chung, JH, Hwang, I, Kwan, YS, Chai, JK, Lee, KH, et al. 2009. Quantification of Quercetin and Kaempferol Contents in Different Parts of Cudrania tricuspidata and Their Processed Foods. *Korean J Hortic Sci* **27**(3): 489-496.

Lai, ED, Teodoro, T, Volchuk, A. 2007. Endoplasmic reticulum stress: Signaling the unfolded protein response. *Physiology* **22**: 193-201.

Lancon, A, Michaille, JJ, Latruffe, N. 2013. Effects of dietary phytophenols on the expression of microRNAs involved in mammalian cell homeostasis. *J Sci Food Agr* **93**(13): 3155-3164.

Lee, IK, Kim, CJ, Song, KS, Kim, HM, Koshino, H, Uramoto, M, et al. 1996. Cytotoxic benzyl dihydroflavonols from Cudrania tricuspidata. *Phytochemistry* **41**(1): 213-216.

Lee, IK, Kim, CJ, Song, KS, Kim, HM, Yoo, ID, Koshino, H, et al. 1995. Two benzylated dihydroflavonols from Cudrania tricuspidata. *Journal of natural products* **58**(10): 1614-1617.

Lee, T, Kwon, J, Lee, D, Mar, W. 2015. Effects of Cudrania tricuspidata Fruit Extract and Its Active Compound, 5,7,3',4'-Tetrahydroxy-6,8-diprenylisoflavone, on the High-Affinity IgE Receptor-Mediated Activation of Syk in Mast Cells. *J Agric Food Chem* **63**(22): 5459-5467.

Liu, Z, Tuo, YH, Chen, JW, Wang, QY, Li, S, Li, MC, et al. 2016. NADPH oxidase inhibitor regulates microRNAs with improved outcome after mechanical reperfusion. *Journal of neurointerventional surgery*.

Lo, J, Patel, VB, Wang, Z, Levasseur, J, Kaufman, S, Penninger, JM, et al. 2013. Angiotensin-converting enzyme 2 antagonizes angiotensin II-induced pressor response and NADPH oxidase activation in Wistar-Kyoto rats and spontaneously hypertensive rats. *Exp Physiol* **98**(1): 109-122.

Lopez-Sepulveda, R, Gomez-Guzman, M, Zarzuelo, MJ, Romero, M, Sanchez, M, Quintela, AM, et al. 2011. Red wine polyphenols prevent endothelial dysfunction induced by endothelin-1 in rat aorta: role of NADPH oxidase. *Clin Sci* **120**(7-8): 321-333.

Mantzaris, MD, Bellou, S, Skiada, V, Kitsati, N, Fotsis, T, Galaris, D. 2016. Intracellular labile iron determines H2O2-induced apoptotic signaling via sustained activation of ASK1/JNK-p38 axis. *Free radical biology & medicine* **97**: 454-465.

Matsuzawa, A, Nishitoh, H, Tobiume, K, Takeda, K, Ichijo, H. 2002. Physiological roles of ASK1-mediated signal transduction in oxidative stress- and endoplasmic reticulum stress-induced apoptosis: Advanced findings from ASK1 knockout mice. *Antioxid Redox Sign* **4**(3): 415-425.

Mkaddem, SB, Pedruzzi, E, Werts, C, Coant, N, Bens, M, Cluzeaud, F, et al. 2010. Heat shock protein gp96 and NAD(P)H oxidase 4 play key roles in Toll-like receptor 4-activated apoptosis during renal

ischemia/reperfusion injury. *Cell Death Differ* **17**(9): 1474-1485.

Mochizuki, T, Furuta, S, Mitsushita, J, Shang, WH, Ito, M, Yokoo, Y, et al. 2006. Inhibition of NADPH oxidase 4 activates apoptosis via the AKT/apoptosis signal-regulating kinase 1 pathway in pancreatic cancer PANC-1 cells. *Oncogene* **25**(26): 3699-3707.

Niizuma, K, Yoshioka, H, Chen, H, Kim, GS, Jung, JE, Katsu, M, et al. 2010. Mitochondrial and apoptotic neuronal death signaling pathways in cerebral ischemia. *Biochimica et biophysica acta* **1802**(1): 92-99.

Nishimura, A, Ago, T, Kuroda, J, Arimura, K, Tachibana, M, Nakamura, K, et al. 2016. Detrimental role of pericyte Nox4 in the acute phase of brain ischemia. *J Cerebr Blood F Met* **36**(6): 1143-1154.

Nomura, Y, Qi, X, Okuma, Y, Hosoi, T. 2004. Edaravone protects against hypoxia/ischemia-induced endoplasmic reticulum dysfunction. *Journal of Pharmacology and Experimental Therapeutics* **311**(1): 388-393.

Olivares, EM, Lwande, W, Delle Monache, F, Bettolo, GM. 1982. A pyrano-isoflavone from seeds of Milletia thonningii. *Phytochemistry* **21**(7): 1763-1765.

Ouyang, YB, Stary, CM, White, RE, Giffard, RG. 2015. The Use of microRNAs to Modulate Redox and Immune Response to Stroke. *Antioxid Redox Sign* **22**(2): 187-202.

Park, HS, Han, KH, Shin, JA, Park, JH, Song, KY, Kim, DH. 2014. The Neuroprotective Effects of Carnosine in Early Stage of Focal Ischemia Rodent Model. *J Korean Neurosurg S* **55**(3): 125-130.

Park, KH, Park, YD, Han, JM, Im, KR, Lee, BW, Jeong, IY, et al. 2006. Anti-atherosclerotic and anti-inflammatory activities of catecholic xanthones and flavonoids isolated from Cudrania tricuspidata. *Bioorganic & medicinal chemistry letters* **16**(21): 5580-5583.

Pedruzzi, E, Guichard, C, Ollivier, V, Driss, F, Fay, M, Prunet, C, et al. 2004. NAD(P)H oxidase Nox-4 mediates 7-ketocholesterol-induced endoplasmic reticulum stress and apoptosis in human aortic smooth

muscle cells. *Mol Cell Biol* **24**(24): 10703-10717.

Perjes, A, Kubin, AM, Konyi, A, Szabados, S, Cziraki, A, Skoumal, R, et al. 2012. Physiological regulation of cardiac contractility by endogenous reactive oxygen species. *Acta physiologica* **205**(1): 26-40.

Ratner, S, Rittenberg, D, Keston, AS, Schoenheimer, R. 1987. The Journal of Biological Chemistry, Volume 134, June 1940: Studies in protein metabolism. XIV. The chemical interaction of dietary glycine and body proteins in rats. By S. Ratner, D. Rittenberg, Albert S. Keston, and Rudolf Schoenheimer. *Nutrition reviews* **45**(10): 310-312.

Sekine, T, Inagaki, M, Ikegami, F, Fujii, Y, Ruangrungsi, N. 1999. Six diprenylisoflavones, derrisisoflavones A–F, from Derris scandens. *Phytochemistry* **52**(1): 87-94.

Siuda, D, Zechner, U, El Hajj, N, Prawitt, D, Langer, D, Xia, N, et al. 2012. Transcriptional regulation of Nox4 by histone deacetylases in human endothelial cells. *Basic Res Cardiol* **107**(5).

Sorce, S, Krause, KH. 2009. NOX enzymes in the central nervous system: from signaling to disease. *Antioxidants & redox signaling* **11**(10): 2481-2504.

Tian, YH, Kim, HC, Cui, JM, Kim, YC. 2005. Hepatoprotective constituents of Cudrania tricuspidata. *Archives of pharmacal research* **28**(1): 44-48.

Truong, DT, Venna, VR, McCullough, LD, Fitch, RH. 2012. Deficits in auditory, cognitive, and motor processing following reversible middle cerebral artery occlusion in mice. *Exp Neurol* **238**(2): 114-121.

Tsao, SCH, Behren, A, Cebon, J, Christophi, C. 2015. The role of circulating microRNA in hepatocellular carcinoma. *Front Biosci-Landmrk* **20**: 78-104.

Vallet, P, Charnay, Y, Steger, K, Ogier-Denis, E, Kovari, E, Herrmann, F, et al. 2005. Neuronal expression of the NADPH oxidase NOX4, and its regulation in mouse experimental brain ischemia. *Neuroscience* **132**(2): 233-238.

Wang, HJ, Huang, YL, Shih, YY, Wu, HY, Peng, CT, Lo, WY. 2014.

MicroRNA-146a Decreases High Glucose/Thrombin-Induced Endothelial Inflammation by Inhibiting NAPDH Oxidase 4 Expression. *Mediat Inflamm*.

Wang, Y, Curtis-Long, MJ, Yuk, HJ, Kim, DW, Tan, XF, Park, KH. 2013. Bacterial neuraminidase inhibitory effects of prenylated isoflavones from roots of Flemingia philippinensis. *Bioorg Med Chem* **21**(21): 6398-6404.

Wissing, F, Smith, JAC. 2000. Vacuolar chloride transport in Mesembryanthemum crystallinum L. measured using the fluorescent dye lucigenin. *J Membrane Biol* **177**(3): 199-208.

Youn, JY, Zhang, J, Zhang, Y, Chen, H, Liu, D, Ping, P, et al. 2013. Oxidative stress in atrial fibrillation: an emerging role of NADPH oxidase. *Journal of molecular and cellular cardiology* **62**: 72-79.

국문 초록

Nox4 mRNA를 표적으로하는 miRNA의 유도를 통한 꾸지뽕나무 열매 추출물과 분리된 컴파운드의 허혈성 손상 세포 및 동물에서의 모델에 대한 신경 보호 효과

홍성은
약학과 천연물과학 전공
서울대학교 약학대학 대학원

퇴행성 뇌질환은 많은 복합적 원인에 의해 발병하는 질환이며 고령화 사회로 인하여 질병의 추이가 계속 높아지고 있다. 뇌졸증으로 인해 발생하는 합병증으로는 편측마비, 안면마비, 구음장애 등이 있으며 치료로 회복하기도 한다. 이에 뇌졸증을 일으키는 원인의 예방도 중요하지만 치료제의 투여로 합병증 및 뇌졸증 치료가 필요한 실정이다. 다음의 연구에서는 천연물질인 꾸지뽕을 이용

하여 뇌졸증 치료제로서의 효과를 입증하고자 하였다.

본 연구에서는 뇌허혈모델인 산소-포도당 결핍(oxygen-glucose deprivation) 과 중뇌동맥협착(middle cerebral artery occlusion)을 통해서 활성산소종(ROS)를 과 발현시키는 Nox4의 억제와 Nox4의 표적 miRNA를 통해 뽕나무 열매의 추출물 FME50과 열매에서 분리된 단일물질인 cudraisoflavone I 와 cudraisoflavone H가 활성산소종을 억제하고 miRNA를 통해 Nox4를 억제 효능을 확인할 수 있는 실험을 진행하였다. 하여 산소-포도당 결핍이 유도된 SH-SY5Y cell 과 흰쥐의 뇌 에서 세포실험과 동물실험을 통해서 꾸지뽕 열매의 추출물 FME50 과 분리된 물질 cudraisoflavone I 와 cudraisoflavone H을 처리한 군의 손상이 농도 구배적으로 회복되어 뇌 신경세포의 보호 효과가 있다는 것을 확인하였다. 또한 소포체 스트레스를 일으키는 외부 원인 중 하나인 활성 산소종(reactive oxygen specis, ROS)의 생성으로 소포체 스트레스에 영향을 주어 세포 사멸의 매게 인자들인 Nox4와 MAPkinas를 활성화 시키며 그에 따른 기전에 대한 규명을 하고자 하였다.

본 연구를 통해 퇴행성 뇌질환의 하나인 허혈성 뇌질환의

치료제의 개발에서 microRNA와 과도한 활성산소종으로 인해 세포 고사를 야기시키며, 세포사멸사를 일으키는 주요한 단백질인 Nox4, ASK1, JNK, p38을 억제하고 허혈/재관류에 의해 유도된 뇌에서의 보호 효과가 있음을 규명하였다.

주요어: 산소 및 포도당 결핍, 허혈/재관류 수술, 허혈성 뇌졸증, 활성 산소종 (ROS), 꾸지뽕, MAPkinase

학 번 : 2014-30572

First Author Publication

PHYTOTHERAPY RESEARCH
Phytother. Res. **31**: 321–329 (2017)
Published online 2 December 2016 in Wiley Online Library
(wileyonlinelibrary.com) **DOI**: 10.1002/ptr.5754

Mulberrofuran G Protects Ischemic Injury-induced Cell Death via Inhibition of NOX4-mediated ROS Generation and ER Stress

Sungeun Hong,[1] Jaeyoung Kwon,[3] Dong-Woo Kim,[1] Hak Ju Lee,[2] Dongho Lee[3]* and Woongchon Mar[1]*

[1]Natural Products Research Institute, College of Pharmacy, Seoul National University, Seoul 08826, Korea
[2]Division of Wood Chemistry and Microbiology, Department of Forest Products, Korea Forest Research Institute, Seoul 02455, Korea
[3]Department of Biosystems and Biotechnology, Korea University, Seoul 02841, Korea

The aim of this study was to investigate the neuroprotective effect of mulberrofuran G (MG) in *in vitro* and *in vivo* models of cerebral ischemia. MG was isolated from the root bark of *Morus bombycis*. MG inhibited nicotinamide adenine dinucleotide phosphate oxidase (NOX) enzyme activity and oxygen–glucose deprivation/reoxygenation (OGD/R)-induced NOX4 protein expression in SH-SY5Y cells. MG inhibited the expression of activated caspase-3 and caspase-9 and cleaved poly adenine dinucleotide phosphate-ribose polymerase in OGD/R-induced SH-SY5Y cells. In addition, MG protected OGD/R-induced neuronal cell death and inhibited OGD/R-induced reactive oxygen species generation in SH-SY5Y cells. In *in vivo* model, MG-treated groups (0.2, 1, and 5 mg/kg) reduced the infarct volume in middle cerebral artery occlusion/reperfusion-induced ischemic rats. The MG-treated groups also reduced NOX4 protein expression in middle cerebral artery occlusion/reperfusion-induced ischemic rats. Furthermore, protein expression of 78-kDa glucose-regulated protein/binding immunoglobulin protein, phosphorylated IRE1α, X-box-binding protein 1, and cytosine enhancer binding protein homologous protein, mediators of endoplasmic reticulum stress, were inhibited in MG-treated groups. Taken together, MG showed protective effect in *in vitro* and *in vivo* models of cerebral ischemia through inhibition of NOX4-mediated reactive oxygen species generation and endoplasmic reticulum stress. This finding will give an insight that inhibition of NOX enzyme activity and NOX4 protein expression could be a new potential therapeutic strategy for cerebral ischemia. Copyright © 2016 John Wiley & Sons, Ltd.

Keywords: mulberrofuran G; neuroprotection; oxygen-glucose deprivation/reoxygenation; middle cerebral artery occlusion/reperfusion; NADPH oxidase; endoplasmic reticulum stress.

INTRODUCTION

Cerebral ischemia is a pathological condition with insufficient blood flow to the brain to meet metabolic demands after acute cerebral infarction or ischemic shock. Oxidative stress damages cellular molecules and leads to neuronal cell death. Many studies have shown that oxidative stress plays a pathological role in cerebral ischemia.

Nicotinamide adenine dinucleotide phosphate (NADPH) oxidase (NOX) has a major role in reactive oxygen species (ROS) generation, and NOX expression is increased after cerebral ischemia. NOX family is composed of seven homologs NOX1, NOX2, NOX3, NOX4, NOX5, DUOX1, and DUOX2. Each member of the NOX family has a different role in cellular biology. NOX is the enzyme complex that is composed of membrane subunits, cytochrome b_{558}, and multiple cytosolic subunits. NOX4 is widely expressed in neurons, astrocytes, and microglia and is activated by the transmembrane subunit of $p22^{phox}$ (Bedard and Krause, 2007). Hence, NOX4 has emerged as a regulator of intracellular ROS and a potential therapeutic strategy in cerebral ischemia (Suzuki *et al.*, 2012). The excessive ROS induces the apoptotic cascade of caspase-3, caspase-9, and poly ADP-ribose polymerase (PARP; Luo *et al.*, 2013).

The increase of cellular stress and oxidative stress can lead to endoplasmic reticulum (ER) stress by activating the process of unfolded protein response. The combination of diverse stresses and excessive ROS production induce the accumulation of unfolded proteins in the ER lumen. When unfolded proteins accumulate in the ER, the molecular chaperone 78-kDa glucose-regulated protein (GRP78), also known as binding immunoglobulin protein (BiP), is dissociated from the three ER membrane receptors. The dissociation of GRP78/BiP from IRE1α, one of ER transmembrane receptors, activates IRE1α by phosphorylation. It triggers IRE1α-mediated ER stress (Wu and Kaufman, 2006). The activated

* Correspondence to: Dongho Lee, Department of Biosystems and Biotechnology, Korea University, Seoul 02841, Korea; Woongchon Mar, Natural Products Research Institute, College of Pharmacy, Seoul National University, Seoul 08826, Korea.
E-mail: dongholee@korea.ac.kr (Dongho Lee); mars@snu.ac.kr (Woongchon Mar)

English language in this manuscript was edited and revised by a professional editorial service, Elsevier Language Editing (Kidlington, UK, http://webshop.elsevier.com).
Supplementary data. The inhibitory effects of MG or VAS2870 on the expression of NOX4 554 mRNA (Fig. S1). The UPLC chromatograms of mulberrofuran G and MeOH extract from the 555 root bark of *M. bombysis* (Fig. S2).

Received 18 March 2016
Revised 19 September 2016
Accepted 07 November 2016

IRE1α splices out a 26-nucleotide intron from the X-box-binding protein 1 (XBP1) mRNA, a transcription factor signaling that produces ER-resident enzymes and chaperones involved in the ER quality control (Calfon *et al.*, 2002). As a consequence of ER stress-induced apoptotic processes, the transcription and translation of cytosine enhancer binding protein homologous protein (CHOP) are increased (Ma *et al.*, 2002). Appearance of CHOP is the final hallmark of ER stress, and its expression is associated with neuronal cell death in cerebral ischemia (McCullough *et al.*, 2001). Many studies have revealed that oxidative stress and ER stress are associated with neuronal cell death signaling after cerebral ischemia.

The *Morus bombycis* Koidz (Moraceae: Morus L) has been reported to contain prenylated flavonoids, benzofurans, and stilbenes with antioxidant, antiinflammatory, and neuronal protective effect (Jin *et al.*, 2006; Kim *et al.*, 2011; Lee *et al.*, 2011). In the previous study, mulberrofuran G (MG) is a prenylated flavonoid and showed antioxidant effect isolated from *Morus nigra* (Abbas *et al.*, 2014) and protected *tert*-butyl hydroperoxide-mediated hepatotoxicity and glutamate-mediated neurotoxicity isolated from *Morus alba* (Jung *et al.*, 2015). In this study, MG from *M. bombycis* evaluated its neuroprotective effects and underlying mechanism in *in vitro* and *in vivo* models of cerebral ischemia.

MATERIALS AND METHODS

Materials. 2′,7′-Dichlorodihydrofluorescein-diacetate (DCFH-DA) and a NOX inhibitor, VAS2870, were purchased from Sigma-Aldrich (St Louis, MO, USA). Dulbecco's modified Eagle's medium (DMEM) and fetal bovine serum were purchased from Gibco BRL (Rockville, MD, USA). Hybond-polyvinylidene difluoride membrane was purchased from Amersham Pharmacia Biotechnology Inc. (Piscataway, NJ, USA). Easy-Blue® total RNA extraction solution, One Step RT-PCR Premix Kits, PRO-PREP protein extraction solution, and WEST-ZOL® ECL solution were purchased from iNtRON Biotechnology (Kyunggi, Korea). NOX4, GRP78/BiP, phosphorylated IRE1α (p-IRE1α), IRE1α, XBP1, CHOP, β-actin primary antibody, and secondary antibody were purchased from Santa Cruz Biotechnology, Inc. (CA, USA).

Preparation of mulberrofuran G. The root bark of *M. bombycis* was collected at Korea Forest Research Institute, Southern Forest Research Center, Jinju, Korea, in September 2008, and authenticated by Dr Hak Ju Lee. A voucher specimen (accession no. MB080911) was deposited at Division of Wood Chemistry and Microbiology, Department of Forest Products, Korea Forest Research Institute, Seoul, Korea.

Isolation of mulberrofuran G. The dried root bark of *M. bombycis* was sliced and extracted with MeOH at room temperature followed by sequential partition with *n*-hexane, $CHCl_3$, and EtOAc. EtOAc-soluble extract (23.9 g) was fractionated on a Sephadex LH-20 column with MeOH to afford seven fractions (Fr 1 to Fr 7). Fr 4 (6.5 g) was chromatographed on a silica gel column with *n*-hexane/acetone (2:1) to give seven fractions (Fr 4.1 to Fr 4.7). Fr 4.4 was applied to a Sephadex LH-20 column with $CHCl_3$/MeOH (1:1) to attain eight fractions (Fr 4.4.1 to Fr 4.4.8); Fr 7 (327.0 mg) was purified by preparative HPLC with MeOH/H_2O (2:3 to 4:1) to obtain MG (18.0 mg, ≥98%). The structure of MG was determined by spectroscopic methods (Geng *et al.*, 2012). Blue amorphous powder; ^{1}H-NMR (500 MHz, CD3OD): δ 1.82 (3H, s, H-7″), 2.05 (1H, d, J = 17.0, 10.5 Hz, H-6″b), 2.69 (1H, dd, J = 17.0, 4.5 Hz, H-6″a), 2.98 (1H, m, H-4″), 3.36 (2H, m, H-3″, H-5″), 6.17 (1H, dd, J = 8.5, 2.5 Hz, H-13″), 6.34 (1H, d, J = 2.0 Hz, H-17″), 6.37 (1H, d, J = 2.5 Hz, H-11″), 6.44 (1H, br s, H-2″), 6.48 (1H, dd, J = 8.0, 2.0 Hz, H-19″), 6.76 (1H, dd, J = 8.5, 2.0 Hz, H-5), 6.85 (1H, br s, H-6′), 6.94 (3H, m, H-3, H-7, H-2′), 7.12 (1H, d, J = 8.0 Hz, H-20″), 7.16 (1H, d, J = 8.5 Hz, H-14″), 7.37 (1H, d, J = 8.5 Hz, H-4); ESI-MS m/z 561 $[M–H]^-$. The purity of the compound was confirmed to be more than 98.0% by HPLC analysis.

Cell culture. The human neuroblastoma cell line SH-SY5Y (ATCC no. CRL-2266) was maintained in DMEM supplemented with 10% heat-inactivated fetal bovine serum and 1% penicillin/streptomycin at 37 °C in a humidified atmosphere of 95% air and 5% CO_2.

Oxygen–glucose deprivation/reoxygenation. Oxygen–glucose deprivation/reoxygenation (OGD/R) was performed as described previously (Cho *et al.*, 2010). Briefly, SH-SY5Y cells were plated in DMEM. After treatment with a compound, the cells were incubated in a hypoxia chamber (Modular Incubator Chamber MIC-101, Billups-Rothenberg, Del Mar, CA) containing a mixture of 95% N_2 and 5% CO_2 at 37% for 16 h. After hypoxia chamber step, the cells were incubated for 24 h for reoxygenation and glucose restoration. In the normoxia control group, the cells were cultured with DMEM containing glucose under normal conditions.

Measurement of cell viability. The SH-SY5Y cells were grown in 96-well culture plates at a density of 2×10^5 cells/200 μL/well for 24 h and then treated with MG (0.016, 0.08, 0.4, and 2 μM), VAS2870, (0.016, 0.08, 0.4, and 2 μM), or vehicle and then exposed to OGD/R conditions. The cell viability was determined by MTT dissolved in phosphate-buffered saline (PBS; 0.5 mg/mL) at 37 °C for 4 h. The formazan crystals were dissolved with dimethyl sulfoxide. The number of viable cells was measured at 540 nm with a microplate reader (SpectraMax® M5; Molecular Devices, Sunnyvale, CA, USA) as previously described (Mosmann, 1983).

Measurement of intracellular reactive oxygen species by flow cytometry. The SH-SY5Y cells were plated into six-well plates at a density of 2×10^5 cells/2 mL/well for 24 h and then cell-treated with MG (0.08, 0.4, and 2 μM), VAS2870 (0.08, 0.4, and 2 μM), or vehicle and then exposed to OGD/R condition. ROS were measured with DCFH-DA, as previously described (Kim

et al., 2015). Briefly, the cells were washed three times with PBS and incubated with DCFH-DA (4 μM) for 30 min at 37 °C in the dark and then washed three times with PBS. Approximately 1×10^4 cells were used for each experiment, and a total of 10 000 events of data were analyzed by CELL QUEST software (BD, San Jose, CA).The fluorescence intensities were measured by flow cytometry (BD FACSCalibur™).

Measurement of nicotinamide adenine dinucleotide phosphate oxidase enzyme activity. The SH-SY5Y cells were plated into six-well plates at a density of 2×10^5 cells/2 mL/well for 24 h and then extracted enzyme. NOX enzyme activity was measured according to a previously described method (Lo *et al.*, 2013). For the NOX enzyme activity assay, SH-SY5Y cells were lysed by sonication at 130 W, frequency 20 Hz, 5 min (Vibra cell-VCX130) in PRO-PREP® protein extraction solution (iNtRON Biotechnology, Korea). The cell lysates were centrifuged at 800 *g* for 10 min at 4 °C. The cell lysates (100-μg protein/100 μL) were incubated with MG (0.016, 0.08, 0.4, 2, 10, and 20 μM), VAS2870 (0.016, 0.08, 0.4, 2, 10, 20, and 50 μM), or vehicle: 10 μM lucigenin, 150 mM of EGTA, 50 mM of sucrose, 100 μM of NADPH, and different concentrations of MG, VAS2870, and vehicle in 96-well white plate. The reaction was performed in the dark for 5 min at room temperature. NOX was measured by a luminometer (Centro LB 960, Berthold Technologies) with lucigenin used as the substrate with an excitation wavelength of 433 nm and an emission wavelength of 506 nm, respectively (Wissing and Smith, 2000).

Protein extraction from oxygen–glucose deprivation/reoxygenation model. The SH-SY5Y cells were plated into six-well culture plates at a density of 1.5×10^5 cells/1 mL/well for 24 h and then cell-treated with MG (0.08, 0.4, and 2 μM), control compound VAS2870 (0.08, 0.4, and 2 μM), or vehicle and exposed to OGD/R conditions. Protein was extracted with PRO-PREP protein extraction solution (iNtRON Biotechnology, Korea) for 20 min at −20 °C. Lysates were centrifuged at 13 000 *g* for 10 min at 4 °C, and the supernatant was used as the protein extract.

Animals. Male Sprague-Dawley rats (230–240 g) were purchased from Samtako Bio Korea (Osan, Korea) and housed in groups (2–3 rats/cage). The environment was maintained at 60% humidity with a 12/12 light–dark cycle and unlimited access to food and water. All animal experiments were approved by the Institutional Animal Care and Use committee of Seoul Nation University and performed in accordance with the requirements of European Directive 2010/63/EU. All efforts were made to minimize the number of animals used and their pain. After each experiment, the animals were euthanized by decapitation after over dose of isoflurane anesthesia.

Animals of treatment. Mulberrofuran G (0.2, 1, and 5 mg/kg) and control compound, carnosine (25, 50, and 75 mg/kg), were dissolved in vehicle (75% propylene glycol in saline) and administered to rats 30 min before middle cerebral artery occlusion/reperfusion (MCAO/R) surgery by the intraperitoneal route. The animals were divided into seven groups of six rats, including sham control group, vehicle group, MG-treated group, and carnosine-treated group.

Middle cerebral artery occlusion experiments/reperfusion. The rats were anesthetized with 2–3% isoflurane (Aerrane®) in a mixture of 30% O_2 and 70% N_2O through a face mask during surgery. Body temperature was maintained at 37 ± 0.5 °C with a heating pad. Focal cerebral ischemia was induced by intraluminal MCAO/R as previously described (Truong *et al.*, 2012). In brief, the right external carotid artery, the common carotid artery, and the internal carotid artery branches were separated from surrounding nerves and fascia. Then, the middle cerebral artery was occluded with a 3-0 poly-L-lysine-coated nylon suture through the extracranial internal carotid artery for 2 h. Reperfusion was performed by removing the suture. The sham-operated control group received all surgical procedures except the suture occlusion. After the MCAO/R surgery, the animals were provided unlimited access to food and water for 24 h. Then, the rats were decapitated after overdose of isoflurane anesthesia.

2,3,5-Triphenyltetrazolium chloride staining and determination of infarct volume. For evaluation the infarct volume, the brains were carefully removed within 3 min of sacrifice. They were cut into five coronal sections of 2-mm thickness by rat brain matrix (Holliston, MA, USA). The slices were placed in 24-well plates and stained with 2% triphenyl tetrazolium chloride at 37 °C for 30 min and then fixed with 4% paraformaldehyde solution. The unstained white area of the brain slice was defined as the infarction, and the infarct volume ratio was measured and calculated by using a computerized image analyzer and IMAGE J software (NIH, Maryland, USA) as previously described (Cho *et al.*, 2010). Briefly, the percentage infarct volume was calculated as $[(V_C - V_L)/V_C] \times 100$, where V_C is the volume of control hemisphere and V_L is the volume of noninfarcted tissue in the lesioned hemisphere.

Protein extraction from middle cerebral artery occlusion/reperfusion model. The cortex was homogenized and then lysed in PRO-PREP protein extraction solution (iNtRON Biotechnology, Korea) for 20 min at −20 °C. The lysates were centrifuged at 13 000 *g* for 10 min at 4 °C, and the supernatant was used as the total brain protein extract.

Western blot analysis. The protein concentration determination was used by Bradford assay (Jones *et al.*, 1989). The equal amounts of protein extracts (15 μg) were separated by electrophoresis on a sodium dodecyl sulfate polyacrylamide gel and, transferred to a polyvinylidene difluoride membrane for 2 h, and then blocked with 5% skim milk in tris-buffered saline with Tween for 2 h at room temperature. The membrane was

incubated overnight at 4 °C with a primary antibody (NOX4, GRP78/BiP, p-IRE1α, IRE1α, XBP1, CHOP, caspase-3, caspase-9, and PARP were diluted 1:2000 and β-actin diluted 1:5000 from 1 mg/mL of stock) followed by incubation with a secondary antibody (anti-rabbit or anti-mouse horseradish peroxidase-conjugated IgG 1:5000 diluted of 1 mg/mL of stock) for 1 h at room temperature. The band intensity was detected by using LAS 4000 (GE Healthcare Life Science, USA) image analyzer. The membrane was stripped and reprobed with anti-IRE1α and anti-β-actin antibody as an internal control as previously described (Ham *et al.*, 2013).

Statistical analysis. All experiments were repeated at least three times and are represented as the mean ± SD. Statistical significance was determined by using GRAPHPAD PRISM (GraphPad Software, CA, USA). The difference among groups was measured by one-way analysis of variance with Bonferroni's multiple comparisons. A value of $p < 0.05$ was considered to be statistically significant.

RESULTS

Protective effect of mulberrofuran G against oxygen–glucose deprivation/reoxygenation-induced cytotoxicity in SH-SY5Y cells

The protective effect of MG (Fig. 1A) against OGD/R-induced neuronal cell death was evaluated by MTT assay within nontoxic concentration ranges. As shown in Fig. 1B, the cell viability of OGD/R-induced group was decreased by 54% compared with that of the normal control group. In contrast, MG (0.016, 0.08, 0.4, and 2 μM) protected against OGD/R-induced cell death in a concentration-dependent manner, with an EC_{50} of 0.58 μM. The NOX inhibitor VAS2870 (0.016, 0.08, 0.4, and 2 μM) protected neuronal cells in a concentration-dependent manner, with an EC_{50} of 0.48 μM.

Inhibitory effect of mulberrofuran G against oxygen–glucose deprivation/reoxygenation-induced intracellular reactive oxygen species generation in SH-SY5Y cells

Intracellular ROS was measured by DCFH-DA. DCFH-DA diffuses through the cell membrane and is deacetylated by cellular esterase. Through this process, DCFH-DA makes its nonfluorescent form, DCFH. DCFH can be rapidly oxidized by intracellular ROS and converts to the highly fluorescent form, dichlorofluorescein (Ratner *et al.*, 1987). As shown in Fig. 1C and D, the OGD/R-induced cells exhibited strong dichlorofluorescein fluorescence intensity compared with the normal control group. The extent of OGD/R-induced ROS production was decreased by MG (0.08–2 μM) in a concentration-dependent manner. NOX inhibitor VAS2870 (0.08–2 μM) also inhibited OGD/R-induced intracellular ROS generation.

Inhibitory effect of mulberrofuran G on nicotinamide adenine dinucleotide phosphate oxidase enzyme activity in whole cell lysates

Nicotinamide adenine dinucleotide phosphate oxidase is a membrane protein that produces superoxide (O_2^-) by

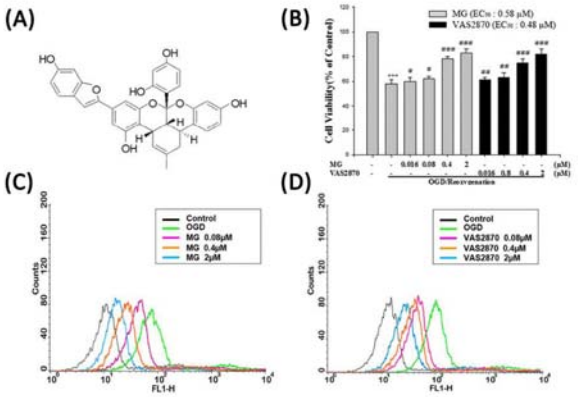

Figure 1. (A) Chemical structure of mulberrofuran G (MG). The effect of MG against oxygen–glucose deprivation/reoxygenation (OGD/R)-induced cell death in SH-SY5Y cells was measured by a 4-methyltrityl reduction assay. (B) The cells were treated with different concentrations of MG (0.016–2 μM) or VAS2870 (0.016–2 μM) and exposed to OGD/R conditions. The effects of MG against OGD/R-induced intracellular reactive oxygen species generation in SH-SY5Y cells are illustrated by 2′,7′-dichlorodihydrofluorescein-diacetate staining and fluorescence-activated cell sorting analyses by using the FL-1 channel. The cells were treated with different concentrations of (C) MG (0.08–2 μM) or (D) VAS2870 (0.08–2 μM) and exposed to OGD/R conditions. Data represent the mean ± SD of three independent experiments ($^{***}p < 0.001$ vs control group, $^{\#}p < 0.05$, $^{\#\#}p < 0.01$, and $^{\#\#\#}p < 0.001$ vs OGD/R-induced group). This figure is available in colour online at wileyonlinelibrary.com/journal/ptr. [Colour figure can be viewed at wileyonlinelibrary.com]

using NADPH as an electron donor. The principle of NOX enzyme activity is that chemiluminescent probe lucigenin is used to indicate the presence of superoxide anion radicals in neuronal cell, and reduced chemiluminescence is detected. We examined the ability of MG to inhibit the lucigenin signal. The inhibitory effect of MG and VAS2870 on NOX enzyme activity was measured by using SH-SY5Y whole cell lysates. As shown in Fig. 2A and B, MG or VAS2870 inhibited NOX enzyme activity with IC_{50} values of 6.9 and 14.5 μM, respectively. The inhibitory potency of NOX enzyme by MG was 2.1-fold higher than that of VAS2870.

Inhibitory effect of mulberrofuran G on endoplasmic reticulum stress-related protein expression in oxygen–glucose deprivation/reoxygenation-induced cell

The inhibitory effect of MG against OGD/R-induced NOX4 protein expression and ER stress was measured by western blot. Under this circumstance, NOX accelerates ROS generation in neuronal cell, and ROS activates ER stress. ER stress markers subsequently induce neuronal cell death and brain injury. As shown in Fig. 2C and D, MG-treated groups (0.08, 0.4, and 2 μM) and VAS2870-treated groups (0.08, 0.4, and 2 μM) decreased NOX4 protein expression. The ER stress-related protein expression was also measured. The protein expression of GRP78/BiP, one of the ER stress markers, was increased after OGD/R induced. MG-treated groups (0.08, 0.4, and 2 μM) showed inhibited protein expression of GRP78/BiP, p-IRE1α, XBP1, and CHOP. VAS2870-treated groups (0.08, 0.4, and 2 μM) also inhibited the ER stress-related protein expression.

Inhibitory effects of mulberrofuran G on the oxygen–glucose deprivation/reoxygenation-induced apoptotic signaling pathway

Caspases initiate cell death by cleavage, which drives the process of apoptosis. Implication of intracellular

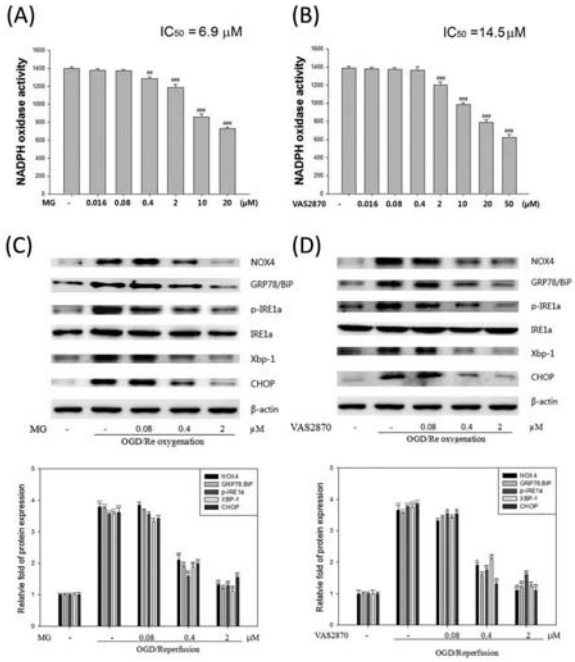

Figure 2. The inhibitory effects of mulberrofuran G (MG) or VAS2870 on nicotinamide adenine dinucleotide phosphate oxidase (NOX) enzyme activity and protein expression of NOX4, 78-kDa glucose-regulated protein/binding immunoglobulin protein (GRP78/BiP), phosphorylated IRE1α (p-IRE1α), IRE1α, X-box-binding protein 1 (XBP1), and cytosine enhancer binding protein homologous (CHOP) protein expression were evaluated by western blot assay. Representative data from three independent experiments are shown. Nicotinamide adenine dinucleotide phosphate oxidase (NOX) enzyme activity in cell lysates was evaluated by using lucigenin after treatment with different concentrations of (A) MG (0.016–20 μM) or (B) VAS2870 (0.016–50 μM). The cells were treated with different concentrations of (C) MG (0.8–2 μM) or (D) VAS2870 (0.8–2 μM) and exposed to oxygen–glucose deprivation/reoxygenation conditions. Data represent the mean ± SD of three independent experiments ($^{***}p < 0.001$ vs control group, $^{\#}p < 0.05$, $^{\#\#}p < 0.01$, and $^{\#\#\#}p < 0.001$ vs oxygen–glucose deprivation/reoxygenation-induced group).

ROS formation induces the cleavage of caspase-9 and caspase-3, and activated caspase-3 cleaves PARP. In this study, the inhibitory effects of MG on the cleaved caspase-9, caspase-3, and PARP were investigated. As shown in Fig. 3A and B, the cleaved caspase-9, caspase-3, and PARP were over-expressed in OGD/R-induced SH-SY5Y cell. However, the over-expression of these cleaved proteins was concentration-dependently decreased by MG and VAS2870 treatment (0.08–2 μM).

Protective effect of mulberrofuran G on cerebral infarction induced by middle cerebral artery occlusion/reperfusion injury

The neuroprotective effect of MG was also evaluated in MCAO/R-induced ischemic rats by measuring the reduction ratio of infarct volume (Fig. 4A). As shown in Fig. 4A, the infarct volumes of MG-treated groups (0.2, 1, and 5 mg/kg) were decreased to 39.0 ± 6.4%, 26.0 ± 7.4%, and 19.0 ± 4.3%, respectively. The infarct volume of vehicle-treated group was 51.2 ± 4.1%. In subsequent experiments, carnosine was used as a control compound. The infarct volumes of carnosine-treated groups (25, 50, and 75 mg/kg) were reduced to 50.6 ± 6.2%, 40.0 ± 6.5%, and 19.6 ± 4.2%, respectively. MG provided a more potent inhibitory effect of brain infarct than carnosine in MCAO/R-induced ischemic rats.

Effect of mulberrofuran G on endoplasmic reticulum stress-related protein expression in the rat model of middle cerebral artery occlusion/reperfusion-induced brain injury

It has been reported that ER stress and NOX activation are generated in MCAO/R-induced brain injury. As shown in Fig. 4B and C, NOX4 protein expression was significantly upregulated in MCAO/R-induced group compared with the sham control group. However, MG-treated groups (0.2, 1, and 5 mg/kg) and carnosine-treated groups (25, 50, and 75 mg/kg) downregulated NOX4 protein expression. The ER stress-related protein GRP78/BiP, p-IRE1α, XBP1, and CHOP expression was also measured. The increased expression of the proteins was inhibited by MG in a concentration-dependent manner (0.2, 1, and 5 mg/kg). Similarly, carnosine decreased the expression of ER stress-related protein in a concentration-dependent manner.

DISCUSSION

The aim of our study was to investigate the neuroprotective effects of MG in *in vitro* and *in vivo* models of cerebral ischemia. We demonstrated that MG significantly inhibited NOX enzyme activity, NOX4 expression, ROS generation, ER stress, apoptosis signal, and neuronal cell death in OGD/R, *in vitro* model of cerebral

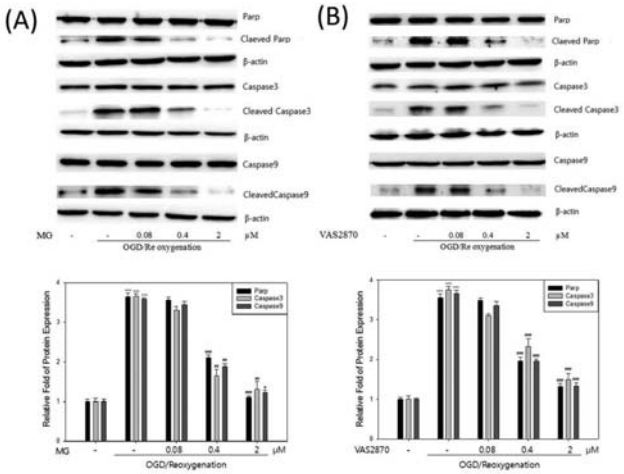

Figure 3. Inhibitory effects of mulberrofuran G (MG) on the expressions of poly adenine dinucleotide phosphate-ribose polymerase (PARP), caspase-3, and cleaved caspase-9 were evaluated by western blot analysis. The cells were treated with different concentrations of (A) MG (0.08–2 μM) or (B) VAS2870 (0.08–2 μM) with oxygen–glucose deprivation (OGD)/reoxygenation-induced group. Data represent the mean ± SD of three independent experiments ($^{***}p < 0.001$ vs control group, $^{\#}p < 0.05$, $^{\#\#}p < 0.01$, and $^{\#\#\#}p < 0.001$ vs oxygen–glucose deprivation/reoxygenation-induced group).

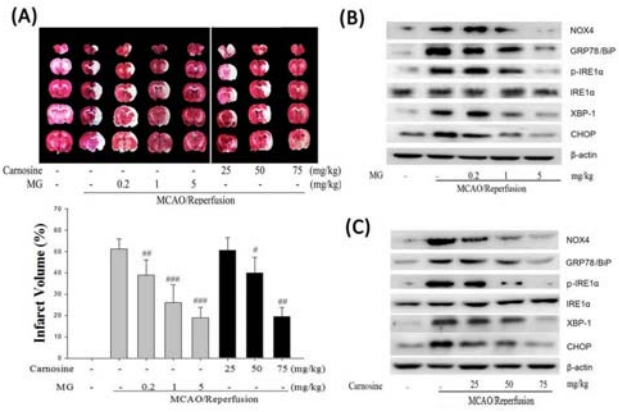

Figure 4. The effects of mulberrofuran G (MG) on the middle cerebral artery occlusion/reperfusion (MCAO/R)-induced cerebral infarct volume in rat brain. Five consecutive, 2-mm-thick slices were stained with triphenyl tetrazolium chloride to visualize the MCAO/R-induced infarct volume in rat brain. The infarct volume ratio in each group was quantified by using IMAGE J software, and each of the quantitative value was shown as a histogram bar with SD value. Representative images of rat brain slices are shown from each group MG (0.2–5 mg/kg) or carnosine (25–75 mg/kg). Data represent the mean ± SD of six independent experiments. (A) The effect of MG on protein expression in MCAO/R-induced rat brain injury. The protein expression of nicotinamide adenine dinucleotide phosphate oxidase type 4 (NOX4), 78-kDa glucose-regulated protein/binding immunoglobulin protein (GRP78/BiP), phosphorylated IRE1α (p-IRE1α), IRE1α, X-box-binding protein 1 (XBP1), cytosine enhancer binding protein homologous protein (CHOP), and β-actin in ischemic cerebrum was evaluated by western blot-treated (B) MG (0.2–5 mg/kg) or (C) carnosine (25–75 mg/kg). Representative images from six independent experiments are shown. [Colour figure can be viewed at wileyonlinelibrary.com]

ischemia. Additionally, MG attenuated ER stress signaling cascades and brain injury in MCAO/R, *in vivo* model of cerebral ischemia.

The brain is particularly susceptible to ischemia, which results in an insufficient supply of oxygen and glucose. In these conditions, the brain activates multiple processes, resulting in neuronal cell death (Graham and Chen, 2001). We focused on NOX4-mediated oxidative stress and CHOP-mediated neuronal cell death during ER stress. Recent studies have suggested that these are potent pathological mechanisms of brain ischemia (Kim *et al.*, 2008), consequently causing irreversible damage to the brain (Wang *et al.*, 2014).

Oxidative stress plays important roles in the pathogenesis of ischemia. The elevated levels of free radicals in the brain cause oxidative damage to organelles and cellular macromolecules (Chan, 2001). Recent research results that NOX4 generates excessive intracellular ROS and it has emerged as an interesting molecule in cerebral ischemia (Chen *et al.*, 2009). On the basis of the previous research about NOX, we suggested that NOX might be a powerful factor in cerebral ischemia. VAS2870 was reported that it is a nonspecific inhibitor for NOX isoforms and suitable for the treatment of ischemic stroke via reducing oxidative stress in OGD/R model (Wingler *et al.*, 2012). In this study, VAS2870 was used as a positive control in OGD/R model. Our results revealed that MG and VAS2870 inhibit NOX enzyme activity with an IC_{50} of 6.9 μM and an IC_{50} of 14.5 μM, respectively, and also decrease NOX4 protein expression in an OGD/R model. MG exerted a 2.1-fold higher inhibitory effect on NOX enzyme activity than VAS2870. A previous study suggested that MG possesses antioxidant effects in the 2,2′-azino-bis-(3-ethylbenzthiazoline-6-sulfonic acid) radical scavenging assay (Abbas *et al.*, 2014). As expected, both MG and VAS2870 inhibited OGD/R-induced ROS generation in SH-SY5Y cells. In this study, it is suggested that the inhibitory effect of MG and VAS2870 on NOX activation is a key role in downregulating excessive ROS generation. MG was also evaluated its ability to protect against OGD/R-induced neuronal cell death by reducing ROS generation via NOX inhibition. MG significantly protected against OGD/R-induced neuronal cell death with an EC_{50} of 0.58 μM, and VAS2870 provided neuronal cell protection with an EC_{50} of 0.48 μM.

It has been reported that carnosine has neuroprotective effects in the early stage of focal ischemia and is a potent hydrophilic antioxidant that protects brain tissues from oxidative injury (Park *et al.*, 2014) and protected ischemic brain damage by inhibiting mitochondrial dysfunction and autophagic process (Baek *et al.*, 2014). In this study, carnosine was used as a positive control in MCAO/R models. Consistent with the results from an OGD/R model of cerebral ischemia, MG prevented rat brain injury by decreasing the MCAO/R-induced infarct volume. The vehicle-treated group had an infarct volume of 51.2 ± 4.1%, whereas a significant decreased infarct volume of 19.0 ± 4.3% was achieved in the MG-treated group (5 mg/kg). The carnosine-treated group (75 mg/kg) had an infarct volume of 19.6 ± 4.2%. MG provided more potent neuroprotection effect against MCAO/R-induced brain injury than carnosine. On the basis of the results of OGD/R-induced neuronal cell death and MCAO/R-induced brain injury, we evaluated the inhibitory effects of MG and VAS2870 on the protein expression of cleaved caspase-9, caspase-3, and PARP, which are the

apoptosis signal factors. OGD/R condition increased the cleaved caspase-9, caspase-3, and PARP protein expression. However, MG and VAS2870 treatment decreased the cleavage of caspase-9, caspase-3, and PARP protein expression. The results suggest that MG inhibits OGD/R-induced apoptosis signal cascade via inhibitory effect of excessive ROS generation and NOX activation.

A growing body of evidence suggests that ER stress is implicated in the pathogenesis of cerebral ischemia brain injury. Recent studies have revealed that oxidative stress and ER stress are associated closely with neuronal cell death signaling after cerebral ischemia (Nakka *et al.*, 2010). During cerebral ischemia, excessive ROS is generated via NOX activation, which induces the accumulation of unfolded proteins in the ER lumen. The accumulation of these unfolded proteins upregulates the expression of the main ER stress regulator, GRP78/BiP, and subsequently induces ER stress (Han *et al.*, 2013). XBP1, one of the ER stress markers, is regulated by p-IRE1α, which increases under ER stress. It was reported that XBP-1 knockout cells have potent neuroprotection against oxidative stress (Liu *et al.*, 2011). Through p-IRE1α-mediated and XBP-1-mediated ER stress, the transcription and translation of CHOP are increased (Ma *et al.*, 2002). The expression of CHOP is a final marker of ER stress and is associated with neuronal cell death and cell cycle arrest in cerebral ischemia (McCullough *et al.*, 2001; Maytin *et al.*, 2001). It has been reported that $CHOP^{-/-}$ mice exhibit reduced apoptosis in response to ER stress presenting smaller infarct volume than wild-type mice when subjected to bilateral carotid artery occlusion (Kohno *et al.*, 1997). Also, CHOP knockout cells were reported to be significantly resistant to ER stress and neuronal cell death. CHOP has been suggested as a major target for therapeutic intervention to prevent the secondary progression of ischemic brain injuries (Oyadomari and Mori, 2004). We investigated the role of MG in protecting neurons from ER stress by determining the protein expression level of CHOP and its related upstream targets, GRP78/BiP, p-IRE1α, and XBP1 in OGD/R and MCAO/R models. MG (0.08–2 μM) and MG (0.2–5 mg/kg) showed a dosage-dependent decrease in the protein expression of GRP78/BiP, p-IRE1α, XBP1, and CHOP. VAS2870 (0.08–2 μM) and carnosine (25–75 mg/kg) also decreased ER stress-related GRP78/BiP, p-IRE1α, XBP1, and CHOP protein expression. Our results suggested that the neurotoxicity mechanism of CHOP-mediated ER stress is inhibited by MG, and decreased CHOP-mediated ER stress prevents OGD/R-induced neuronal cell death and MCAO/R-induced brain injury.

This study demonstrated that MG suppressed NOX4 protein expression, ROS generation, ER stress, and apoptosis signal and protects against neuronal cell death in an OGD/R model. Also, MG inhibited NOX enzyme activity. These inhibitory effects on ROS and NOX resulted in significant reduction in the infarct volume of MCAO/R-induced brain injuries and decreased protein expression of ER stress markers such as GRP78/BiP, p-IRE1α, XBP1, and CHOP. Taken together, our data reveal that the neuroprotective mechanisms of MG are the inhibition of CHOP-mediated ER stress-induced apoptosis as well as ROS generation via inhibiting NOX activity. It suggests that MG can be a useful candidate for the treatment of ischemic brain diseases.

Acknowledgements

This work was supported by the Basic Science Research Program through the National Research Foundation (NRF) of Korea (grant no. NRF-2013R1A1A2008111) and the BK21 plus program in 2016 through the National Research Foundation (NRF) funded by the Ministry of Education of Korea. The author appreciates Korea University and the Korea Forest Research Institute for supporting the plant materials.

Conflict of Interest

The authors have declared that there are no conflicts of interest.

REFERENCES

Abbas GM, Bar FMA, Baraka HN, Gohar AA, Lahloub MF. 2014. A new antioxidant stilbene and other constituents from the stem bark of *Morus nigra* L. *Nat Prod Res* **28**: 952–9.

Baek SH, Noh AR, Kim KA, *et al.* 2014. Modulation of mitochondrial function and autophagy mediates carnosine neuroprotection against ischemic brain damage. *Stroke* **45**: 2438–43.

Bedard K, Krause KH. 2007. The NOX family of ROS-generating NADPH oxidases: physiology and pathophysiology. *Physiol Rev* **87**: 245–313.

Calfon M, Zeng H, Urano F, *et al.* 2002. IRE1 couples endoplasmic reticulum load to secretory capacity by processing the XBP-1 mRNA. *Nature* **415**: 92–6.

Chan PH. 2001. Reactive oxygen radicals in signaling and damage in the ischemic brain. *J Cereb Blood Flow Metab* **21**: 2–14.

Chen H, Song YS, Chan PH. 2009. Inhibition of NADPH oxidase is neuroprotective after ischemia–reperfusion. *J Cereb Blood Flow Metab* **29**: 1262–72.

Cho EY, Lee SJ, Nam KW, *et al.* 2010. Amelioration of oxygen and glucose deprivation-induced neuronal death by chloroform fraction of bay leaves (*Laurus nobilis*). *Biosci Biotechnol Biochem* **74**: 2029–35.

Geng CA, Ma YB, Zhang XM, *et al.* 2012. Mulberrofuran G and isomulberrofuran G from *Morus alba* L.: anti-hepatitis B virus activity and mass spectrometric fragmentation. *J Agric Food Chem* **60**: 8197–202.

Graham SH, Chen J. 2001. Programmed cell death in cerebral ischemia. *J Cereb Blood Flow Metab* **21**: 99–109.

Ham A, Kim DW, Kim KH, *et al.* 2013. Reynosin protects against neuronal toxicity in dopamine-induced SH-SY5Y cells and 6-hydroxydopamine-lesioned rats as models of Parkinson's disease: reciprocal up-regulation of E6-AP and down-regulation of alpha-synuclein. *Brain Res* **1524**: 54–61.

Han J, Murthy R, Wood B, *et al.* 2013. ER stress signalling through eIF2alpha and CHOP, but not IRE1alpha, attenuates adipogenesis in mice. *Diabetologia* **56**: 911–24.

Jin YS, Lee MJ, Han W, Heo SI, Sohn SI, Wang MH. 2006. Antioxidant effects and hepatoprotective activity of 2,5-dihydroxy-4,3′-di(beta-D-glucopyranosyloxy)-trans-stilbene *Morus bombycis* Koidzumi roots on CCl4-induced liver damage. *Free Radic Res* **40**: 986–92.

Jones CG, Hare JD, Compton SJ. 1989. Measuring plant protein with the Bradford assay. 1. Evaluation and standard method. *J Chem Ecol* **15**: 979–92.

Jung JW, Ko WM, Park JH, *et al.* 2015. Isoprenylated flavonoids from the root bark of *Morus alba* and their hepatoprotective and neuroprotective activities. *Arch Pharm Res* **38**: 2066–75.

Kim DW, Lee KT, Kwon J, Lee HJ, Lee D, Mar W. 2015. Neuroprotection against 6-OHDA-induced oxidative stress and apoptosis in SH-SY5Y cells by 5,7-dihydroxychromone: activation of the Nrf2/ARE pathway. *Life Sci* **130**: 25–30.

Kim HS, Kim AR, Park HJ, *et al.* 2011. *Morus bombycis* Koidzumi extract suppresses collagen-induced arthritis by inhibiting the activation of nuclear factor-kappa B and activator protein-1 in mice. *J Ethnopharmacol* **136**: 392–8.
Kim I, Xu W, Reed JC. 2008. Cell death and endoplasmic reticulum stress: disease relevance and therapeutic opportunities. *Nat Rev Drug Discov* **7**: 1013–30.
Kohno K, Higuchi T, Ohta S, Kohno K, Kumon Y, Sakaki S. 1997. Neuroprotective nitric oxide synthase inhibitor reduces intracellular calcium accumulation following transient global ischemia in the gerbil. *Neurosci Lett* **224**: 17–20.
Lee HJ, Lyu DH, Koo U, *et al.* 2011. Inhibitory effect of 2-arylbenzofurans from the Mori Cortex Radicis (Moraceae) on oxygen glucose deprivation (OGD)-induced cell death of SH-SY5Y cells. *Arch Pharm Res* **34**: 1373–80.
Liu Y, Zhang X, Liang Y, *et al.* 2011. Targeting X box-binding protein-1 (XBP1) enhances sensitivity of glioma cells to oxidative stress. *Neuropathol Appl Neurobiol* **37**: 395–405.
Lo J, Patel VB, Wang Z, *et al.* 2013. Angiotensin-converting enzyme 2 antagonizes angiotensin II-induced pressor response and NADPH oxidase activation in Wistar–Kyoto rats and spontaneously hypertensive rats. *Exp Physiol* **98**: 109–22.
Luo Y, Yang X, Zhao S, *et al.* 2013. Hydrogen sulfide prevents OGD/R-induced apoptosis via improving mitochondrial dysfunction and suppressing an ROS-mediated caspase-3 pathway in cortical neurons. *Neurochem Int* **63**: 826–31.
Ma Y, Brewer JW, Diehl JA, Hendershot LM. 2002. Two distinct stress signaling pathways converge upon the CHOP promoter during the mammalian unfolded protein response. *J Mol Biol* **318**: 1351–65.
Maytin EV, Ubeda M, Lin JC, Habener JF. 2001. Stress-inducible transcription factor CHOP/gadd153 induces apoptosis in mammalian cells via p38 kinase-dependent and -independent mechanisms. *Exp Cell Res* **267**: 193–204.
Mccullough KD, Martindale JL, Klotz LO, Aw TY, Holbrook NJ. 2001. Gadd153 sensitizes cells to endoplasmic reticulum stress by down-regulating Bcl2 and perturbing the cellular redox state. *Mol Cell Biol* **21**: 1249–59.
Mosmann T. 1983. Rapid colorimetric assay for cellular growth and survival — application to proliferation and cyto-toxicity assays. *J Immunol Methods* **65**: 55–63.
Nakka VP, Gusain A, Raghubir R. 2010. Endoplasmic reticulum stress plays critical role in brain damage after cerebral ischemia/reperfusion in rats. *Neurotox Res* **17**: 189–202.
Oyadomari S, Mori M. 2004. Roles of CHOP/GADD153 in endoplasmic reticulum stress. *Cell Death Differ* **11**: 381–9.
Park HS, Han KH, Shin JA, Park JH, Song KY, Kim DH. 2014. The neuroprotective effects of carnosine in early stage of focal ischemia rodent model. *J Korean Neurosurg Soc* **55**: 125–30.
Ratner S, Rittenberg D, Keston AS, Schoenheimer R. 1987. The journal of biological chemistry, volume 134, June 1940: studies in protein metabolism. XIV. The chemical interaction of dietary glycine and body proteins in rats. By S. Ratner, D. Rittenberg, Albert S. Keston, and Rudolf Schoenheimer. *Nutr Rev* **45**: 310–2.
Suzuki Y, Hattori K, Hamanaka J, *et al.* 2012. Pharmacological inhibition of TLR4-NOX4 signal protects against neuronal death in transient focal ischemia. *Sci Rep* **2**: 896.
Truong DT, Venna VR, Mccullough LD, Fitch RH. 2012. Deficits in auditory, cognitive, and motor processing following reversible middle cerebral artery occlusion in mice. *Exp Neurol* **238**: 114–21.
Wang N, Zhang Y, Wu L, *et al.* 2014. Puerarin protected the brain from cerebral ischemia injury via astrocyte apoptosis inhibition. *Neuropharmacology* **79**: 282–9.
Wingler K, Altenhoefer SA, Kleikers PWM, Radermacher KA, Kleinschnitz C, Schmidt HHHW. 2012. VAS2870 is a pan-NADPH oxidase inhibitor. *Cell Mol Life Sci* **69**: 3159–60.
Wissing F, Smith JC. 2000. Vacuolar chloride transport in *Mesembryanthemum crystallinum* L. measured using the fluorescent dye lucigenin. *J Membr Biol* **177**: 199–208.
Wu J, Kaufman RJ. 2006. From acute ER stress to physiological roles of the unfolded protein response. *Cell Death Differ* **13**: 374–84.

SUPPORTING INFORMATION

Additional supporting information may be found in the online version of this article at the publisher's web site.